Hindawi
Geofluids
Volume 2023, Article ID 8840352, 28 pages
https://doi.org/10.1155/2023/8840352

Research Article

Heat Transfer Analysis of Enhanced Geothermal System Based on Heat-Fluid-Structure Coupling Model

Linchao Wang,[1] Xin Liang,[1] Xuyang Shi,[2] Jianyong Han,[3] Yang Chen,[1] and Wan Zhang[1]

[1]*School of Civil Engineering and Architecture, Xi'an University of Technology, Xi'an 710048, China*
[2]*School of Mechanics and Civil Engineering, China University of Mining and Technology, Xuzhou 221116, China*
[3]*School of Civil Engineering, Shandong Jianzhu University, Jinan 250101, China*

Correspondence should be addressed to Xin Liang; xliang@xaut.edu.cn and Xuyang Shi; sxywlp2008@163.com

Received 15 August 2023; Revised 18 October 2023; Accepted 28 October 2023; Published 16 November 2023

Academic Editor: Qingchao Li

Dry hot rock geothermal resources by virtue of its wide distribution, large reserves, clean and low-carbon, stable, high utilization rate, and other characteristics have been widely used. The enhanced geothermal system (EGS) is the most efficient approach for harnessing and exploiting geothermal energy from hot, arid rock formations. To investigate the impact of varying parameters on heat recovery in EGS operations, we employed the COMSOL numerical simulation software to construct a seepage heat transfer model for fractured rock masses. Essential parameters and boundary conditions were established, followed by conducting numerical simulations. Through the numerical simulation results, the temporal and spatial changes of coupling effects among seepage field, stress field, and temperature field in fractured rock mass were analyzed. We investigated the impact of water injection temperature, injection-production pressure difference, injection flow rate, and initial reservoir temperature on the heat transfer process. The findings indicate that raising the water injection temperature and injection-production pressure difference can enhance the reservoir's heat recovery capability. However, it may also accelerate thermal breakthrough and reduce the system's operational lifespan. The higher injection flow rate can improve the heat recovery efficiency. However, too large injection flow can cause problems in other aspects of the reservoir; increasing reservoir temperature leads to higher production temperatures, which can potentially result in dynamic catastrophes. Therefore, while ensuring the heat recovery efficiency of the system, the operation life of the system can be extended by adjusting the water injection temperature in stages, setting a reasonable injection and production pressure difference, and selecting an appropriate injection flow rate, so as to achieve the purpose of EGS optimization.

1. Introduction

Since the beginning of the Industrial Revolution, the rapid development of industries worldwide has led to a sharp increase in the demand for fossil fuels, resulting in a significant amount of greenhouse gas emissions and global warming [1, 2]. As a result, the search for and development of renewable energy to replace fossil fuels have become new directions for countries to formulate their energy strategies [3]. Geothermal energy, with its advantages of cleanliness, low carbon emissions, abundant resources, stable and reliable supply, direct utilization without conversion, and high efficiency, has gained broad recognition from countries around the world [4]. Geothermal energy is regarded as a highly promising renewable energy source for the future, given its vast development potential and widespread resource distribution [5–7].

Geothermal energy can be classified into two types based on storage form: hydrothermal and hot dry rock (HDR) [8]. Hydrothermal geothermal resources refer to underground

water reservoirs in the form of hot fluids [9], while HDR geothermal resources are deep-seated rock formations located 3-10 km underground with temperatures usually exceeding 200°C. Due to their high-temperature characteristics, HDR geothermal resources are widely used in the field of power generation and have tremendous development potential and economic value [10]. The characteristics of HDR include high temperature, wide distribution range, and large burial depth. HDR almost lacks or has only a small amount of fluid, and the rock formation itself is highly dense with extremely low permeability. In order to develop HDR geothermal resources, enhanced geothermal systems (EGS) have been constructed [11–13].

EGS is generally used for the development and utilization of HDR. First, the exploited HDR reservoir is transformed into an artificial geothermal reservoir. A low-temperature working fluid is injected into the injection well, where it flows through the artificial geothermal reservoir. During this process, heat exchange occurs between the low-temperature working fluid and the high-temperature rock formation surrounding the fractures [14–17]. The heated working fluid is then pumped out of the production well, completing the circulation process [18]. Therefore, EGS systems face many complex engineering and scientific problems, such as establishing models for thermal reservoirs, studying the multifield coupling of fractured rock formations in thermal reservoirs, and evaluating and predicting the thermal extraction performance of reservoirs. In order to enhance the practical applications of EGS systems, it is necessary to conduct comprehensive research and develop effective solutions for these challenges [19, 20].

In the 1970s, Los Alamos National Laboratory in the United States took the lead in conducting research on HDR development and accumulated valuable experience in HDR development as the research progressed [21]. From the 1980s to the 1990s, several developed countries successively carried out experiments and research on HDR drilling and exploitation technologies [22, 23]. In 1973, the United States launched the world's first EGS demonstration project, which proved the feasibility of forming a geothermal reservoir in HDR through geological and drilling techniques [24]. In 1974, Japan initiated a project to study HDR power generation technology [25]. By conducting experimental research on deep high-temperature HDR and using methods such as hydraulic fracturing and proppant placement, an artificial thermal reservoir was established, and HDR power plants were built in the early 21st century [26]. To enhance heat transfer efficiency and production yield, France conducted efforts to improve hydraulic and chemical stimulation of the thermal reservoir between the injection well and the production well. The world's first successful HDR power plant was established in the Soultz area in 1987 after drilling tests and hydraulic fracturing experiments, and it is still in operation today [27]. In the early 21st century, the United States launched research called "Enhanced Geothermal Systems" and initially established geological exploration, engineering fracturing, and development and utilization technical specifications for EGS [28]. In 2003, Australia conducted detailed surveys of the Cooper Basin and established a relevant EGS research program, with results showing that the temperature of HDR buried at a depth of about 4,500 meters can reach 270°C [29].

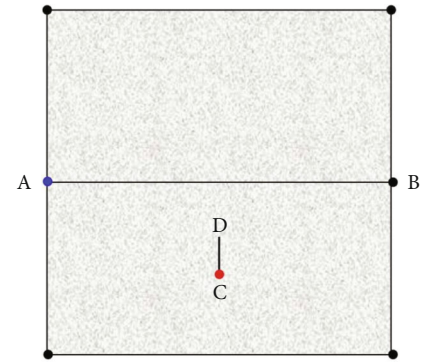

Figure 1: Seepage heat transfer model of fractured rock mass.

To solve the simulation problems of EGS, many scholars have developed effective models to simulate the performance of EGS [30–32]. Zhang et al. [33] constructed a mathematical model for porous media with single fractures to simulate the thermohydrological coupling process in heat exchange within EGS. Chen et al. [34] introduced a discrete fracture network into the matrix rock mass to simulate fluid flow and heat transfer processes. Jiang et al. [35] proposed a three-dimensional transient model that takes into account the presence of local thermal imbalances between the rock matrix and fluid flow in porous thermal reservoirs. Shaik et al. [36] developed a numerical simulation program that couples fluid flow with matrix rock and circulating fluid heat transfer for geothermal systems with natural fractures, which is closer to the dynamic changes of fractures in the thermal extraction process of EGS under realistic conditions. Baria et al. [37] established a self-supporting single fracture T-H-M coupling model based on cavity elasticity theory. Wang et al. [38] introduced the concept of strong discontinuity into the DFN model to simulate the thermal production process of geothermal reservoirs and capture the aperture changes of each fracture caused by fluid pressure, external stress, and thermal expansion during production. Asai et al. [39] studied the influence of different injection flow rates on dual-well EGS and proposed an exponential flow scheme as the optimal solution.

Compared to the traditional heat transfer medium H_2O, CO_2 has a lower critical pressure and critical temperature. Additionally, the dynamic viscosity of liquid CO_2 is much smaller than that of water. The utilization of CO_2 as an alternative to water for geothermal energy extraction was initially suggested by Brown [40]. Moreover, CO_2 can also be used as a heat transfer medium for underground CO_2 storage, achieving carbon capture. Pruess [41, 42] used TOUGH2 software to establish heat extraction models for EGS using both H_2O and CO_2, based on basic data from the Soultz region in France. Through a comparison and analysis of heat extraction efficiency, the findings indicated that CO_2 as a working fluid demonstrates approximately twice the heat extraction efficiency compared to H_2O. Nevertheless, it should be noted that CO_2 as a working fluid suffers from

Table 1: Model correlation parameters.

Parameters (unit)	Parameter value	Parameters (unit)	Parameter value
Poisson's ratio	0.25	Thermal conductivity (W/(m·K))	5
Porosity	0.01	Specific heat rate	1
Permeability (m^2)	1×10^{-15}	Densities (kg/m^3)	2500
Young's modulus	3×10^{10}	Constant pressure heat capacity (J/(kg·K))	800
Initial reservoir temperature (°C)	100	Water injection temperature (°C)	20
Initial reservoir pressure (Pa)	2×10^7	Injection well pressure (Pa)	4×10^7
Production well pressure (Pa)	1×10^7	Injection flow (m^3/s)	0.02

the drawback of poor stability. During the operation of EGS, CO_2 can cause salt precipitation and potential blockage, leading to a decrease in heat extraction efficiency [43].

This article is grounded in the theory of coupled heat-mass transfer, taking into account the interactions of deformation, seepage, heat transfer within the matrix rock, and fractures. Moreover, numerical simulations are performed by varying the physical parameters of EGS to assess their influence on the heat transfer process and propose optimization strategies for enhancing EGS performance.

2. Mathematical Models and Numerical Simulations

2.1. Numerical Simulation Software. To solve the coupled theory equations of heat-flow-solid in the mathematical model, the software used is COMSOL Multiphysics 5.6, developed by a company in Stockholm, Sweden. This software is capable of conducting multiphysics coupling analysis and possesses strong numerical computing capabilities. It has been recognized by many scholars as the "first truly arbitrary multiphysics coupling analysis software" and holds a significant position in the field of multiphysics coupling. Compared to other finite element analysis software, it is more flexible, user-friendly, and easy to learn. COMSOL Multiphysics is based on the finite element analysis principle and does not require the presetting of finite elements. It reverts the finite element method to the most fundamental variational level in the field of mathematics. By solving a system of partial differential equations, it achieves the coupled solution of multiple physics fields, allowing for full coupling and greater proximity to reality. In this study, the heat transfer module, Darcy's module, and solid mechanics module within COMSOL were employed. Customized configurations were implemented to establish the interconnections among these modules, facilitating their coupling for comprehensive analysis.

2.2. Model Assumptions. In general, the permeability of hot dry rocks is extremely low, almost close to zero. By using hydraulic fracturing, a network of fractures is created in the reservoir of hot dry rocks to increase the permeability. In this process, low-temperature water is injected through injection wells, and as water flows along the fractures, it simultaneously absorbs heat from the surrounding rock.

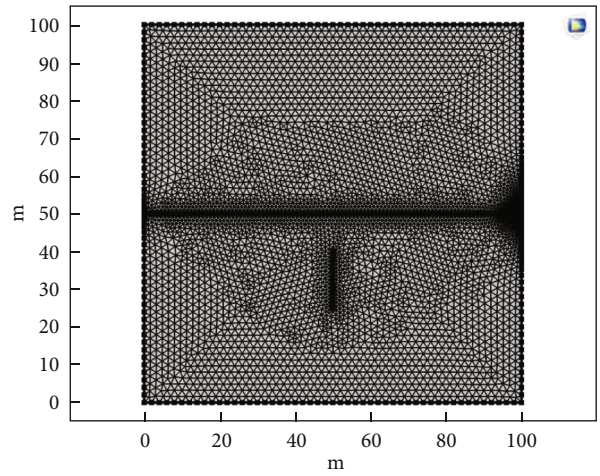

Figure 2: Fracture grid division diagram.

Finally, high-temperature water is extracted from production wells. This process involves the coupling of three complex spatiotemporal phenomena: temperature field (T), flow field (H), and stress field (M). To gain a comprehensive understanding of the coupled interactions within an enhanced geothermal system (EGS), it is necessary to develop a mathematical model. In order to simplify the analysis, the following assumptions have been considered:

(1) Hot dry rocks are a continuous isotropic porous medium

(2) The fracture surfaces in the reservoir extend infinitely, and the width of fractures is much smaller than their length

(3) The rock matrix is treated as a homogeneous porous medium with significantly lower permeability compared to fractures. The primary flow pathways for fluids are considered to be the surfaces of fractures

(4) The flow of water follows Darcy's law

(5) Heat transfer between water and the surrounding rock is achieved through convection and conduction

(6) Chemical reactions that may occur between fluid and hot dry rock are ignored

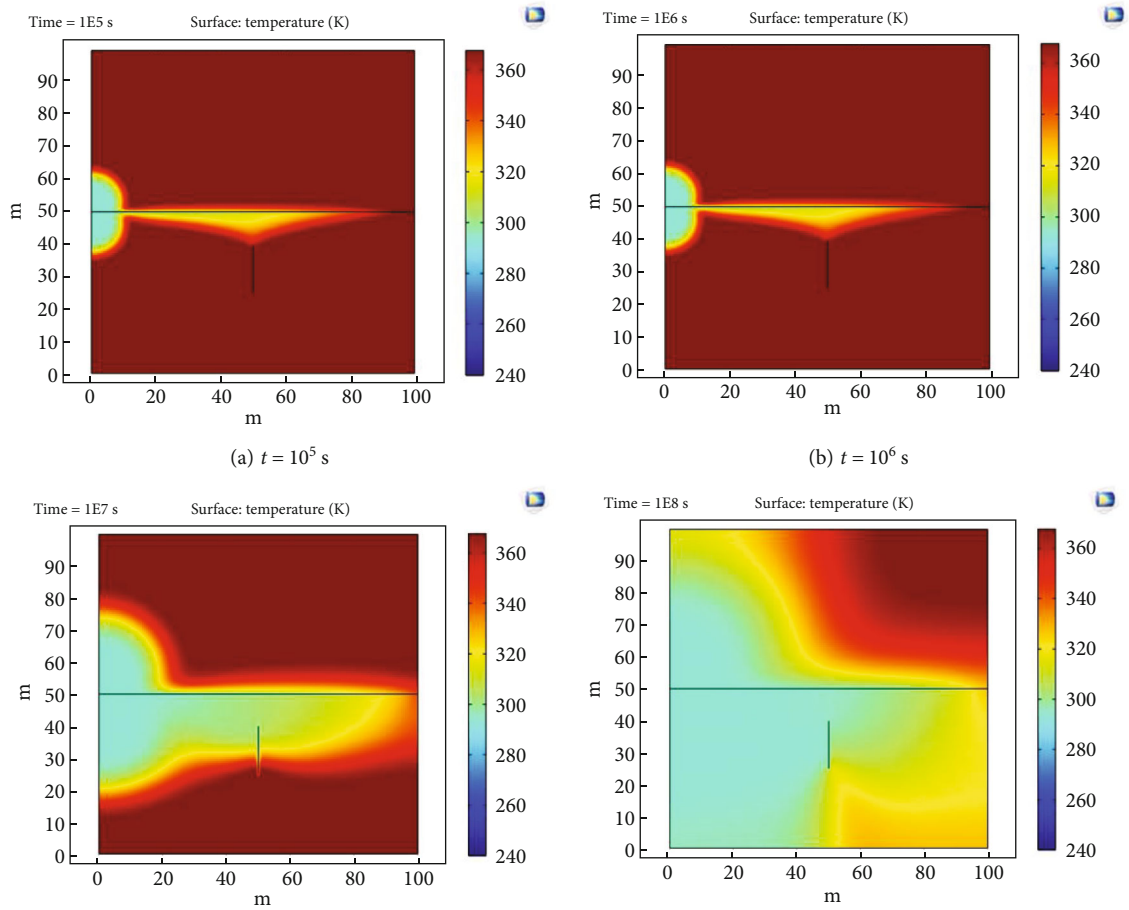

(a) $t = 10^5$ s (b) $t = 10^6$ s

(c) $t = 10^7$ s (d) $t = 10^8$ s

Figure 3: Temperature field cloud image of fractured rock mass ($T = 293.15$ K).

(7) The fluid remains in a liquid state even under high pressure

2.3. Primary Governing Equations

2.3.1. Equations for the Rock Permeability Field.

$$\begin{cases} S\dfrac{\partial p}{\partial t} + \nabla \cdot u = -\dfrac{\partial e}{\partial t} + Q, \\ u = -\dfrac{k}{\eta}(\nabla p + \rho g \nabla z), \end{cases} \tag{1}$$

where S represents the storativity coefficient, t represents time, u represents the water flow velocity in the rock matrix, e is the volumetric strain of the rock, and Q represents the source/sink term for fluid flow. k denotes the permeability of the rock mass, while η represents the dynamic viscosity of the fluid.

2.3.2. Equations for the Rock Stress Field.

$$\begin{cases} \sigma_{\mathrm{ij},j} + F_i = 0, \\ \mu u_{i,\mathrm{ij}} + (\lambda + \mu) u_{j,\mathrm{ij}} - \alpha_B p_{,i} - \beta_T T_{s,i} + F_i = 0, \\ \mu = \dfrac{E}{2(1+\nu)}, \\ \lambda = \dfrac{E\nu}{[(1+\nu)(1-2\nu)]}, \\ \beta_T = \dfrac{\alpha_T E}{(1-2\nu)}, \end{cases} \tag{2}$$

where $\sigma_{ij,j}$ represents the components of the stress tensor, F_i is the body force, u is the displacement, λ and μ are the Lamé constants, p is the pore pressure, α_B is the Biot consolidation coefficient, T_s is the rock temperature, β_T is the thermal expansion factor, and $\alpha_B p_{,i}$ and $\beta_T T_{s,i}$, respectively, represent the terms for the effects of pore pressure and temperature on stress. E is the elastic modulus, and α_T is the thermal expansion coefficient.

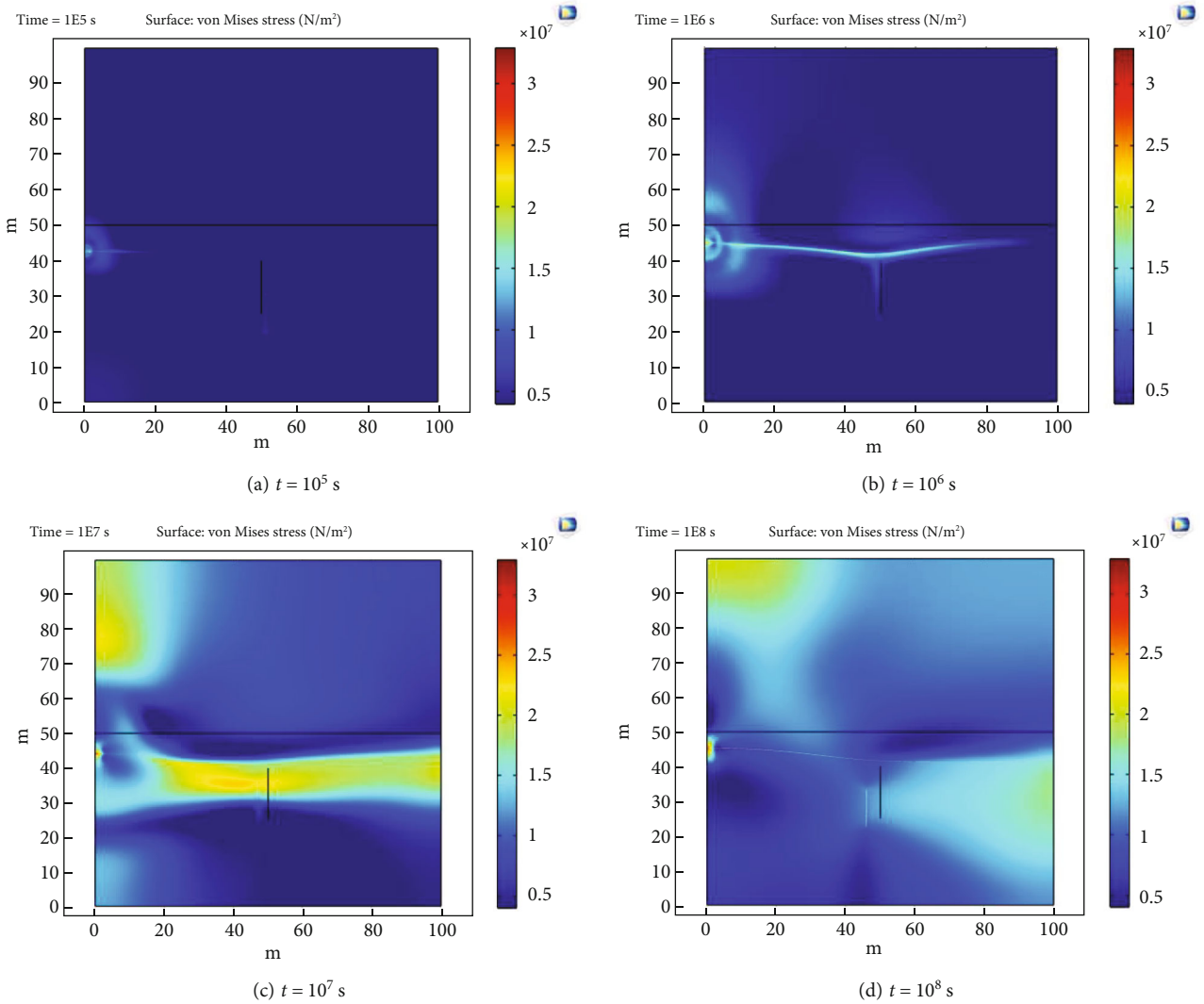

(a) $t = 10^5$ s

(b) $t = 10^6$ s

(c) $t = 10^7$ s

(d) $t = 10^8$ s

Figure 4: Cloud map of stress field of fractured rock mass ($T = 293.15$ K).

2.3.3. Equation for the Rock Temperature Field.

$$c_s \rho_s \frac{\partial T_s}{\partial t} = \lambda_s \nabla^2 T_s + W, \tag{3}$$

where c_s is the specific heat capacity of the rock, ρ_s is the density of the rock, λ_s is the thermal conductivity of the rock, and W represents the heat source.

2.3.4. Equations for the Fracture Permeability Field.

$$d_f S_f \frac{\partial p}{\partial t} + \nabla_\tau \cdot \left(-d_f \frac{k_f}{\eta} \nabla p \right) = -d_f \frac{\partial e_f}{\partial t} - \frac{k_f}{\eta} \frac{\partial p}{\partial n}, \tag{4}$$

where d_f is the width of the fracture aperture, S_f is the storativity coefficient of the fracture, ∇_τ represents the derivative along the tangential direction of the fracture, k_f is the permeability of the fracture, e_f is the volumetric strain of the fracture surface, and n represents the normal vector of the fracture surface.

2.3.5. Equations for the Fracture Stress Field.

$$\begin{cases} u_n = \dfrac{\sigma_n'}{k_n}, \\ u_s = \dfrac{\sigma_s'}{k_s}, \\ \sigma_n' = \sigma_n - p, \\ \sigma_s' = \sigma_s, \end{cases} \tag{5}$$

where u represents the displacement, σ' is the effective stress, k represents the stiffness, and the subscripts n, s represent the normal and tangential directions, respectively.

2.3.6. Equation for the Fracture Temperature Field.

$$d_f \rho_f c_f \frac{\partial T_f}{\partial t} + d_f \rho_f c_f u_f \nabla_\tau T_f = d_f \nabla_\tau \cdot \left(\lambda_f \nabla_\tau T_f \right), \tag{6}$$

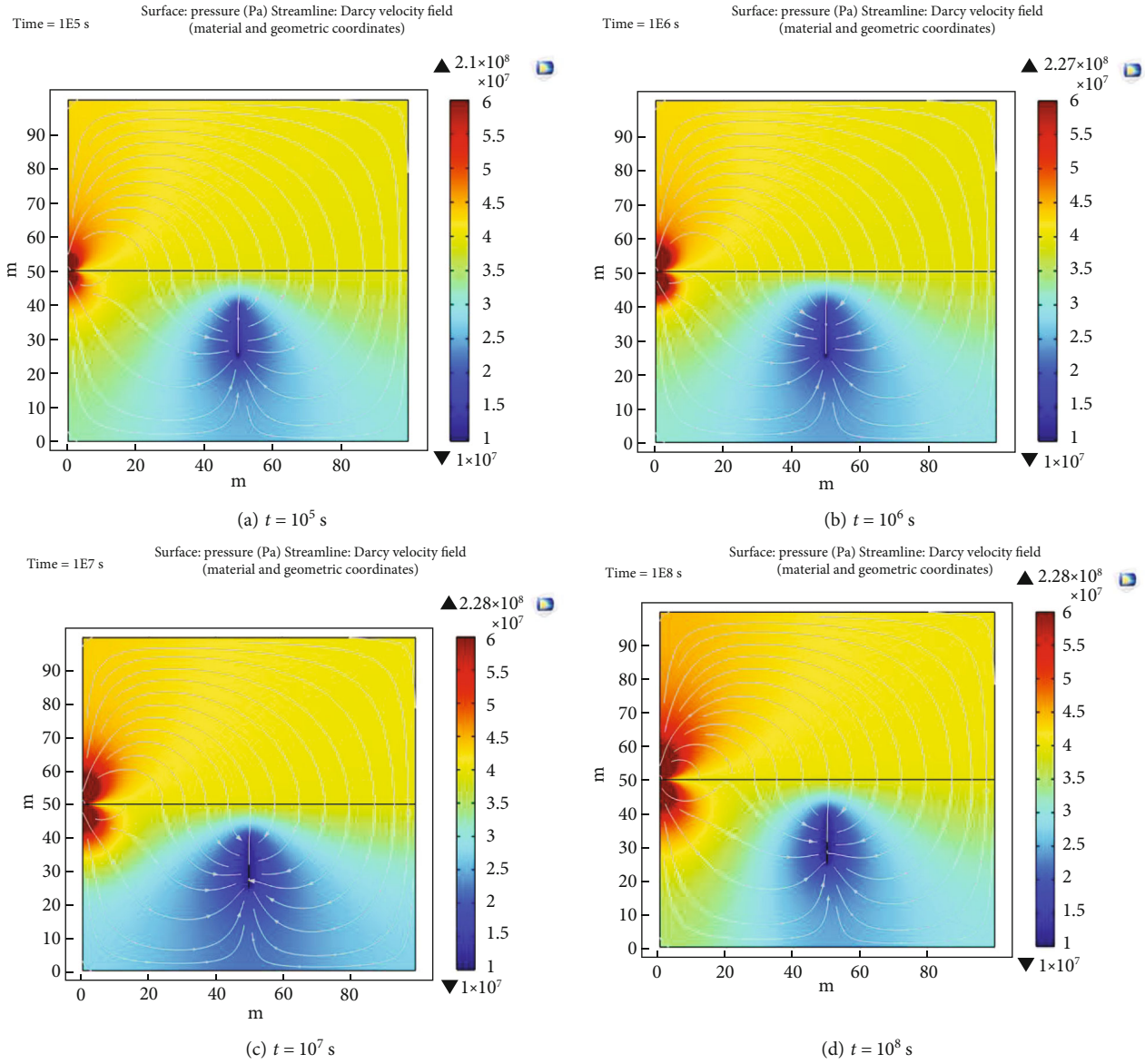

Figure 5: Cloud map of seepage field of fractured rock mass ($T = 293.15$ K).

where ρ_f is the density of water, c_f is the specific heat capacity of water, u_f is the velocity of water flow within the fracture, and λ_f is the thermal conductivity of water.

2.4. Numerical Simulation

2.4.1. Model Description. Hot rock formations refer to underground rock layers with high temperatures, typically increasing by 10-30 degrees Celsius per kilometer in depth. These rocks are rich in minerals such as quartz, feldspar, and mica, as well as rocks with high thermal conductivity, such as granite, basalt, and schist. The thermal conductivity of the rocks determines the speed and efficiency of heat transfer within the rocks. Hot rock formations are usually found at greater depths underground and are subjected to higher geological stress, which can cause fractures in the rocks or affect the permeability of the thermal water or heat-conducting medium. To better simulate the real conditions of dry hot rocks, this study developed a model for fluid flow and heat transfer.

Fractured rock mass seepage and heat transfer model is shown in Figure 1. The thermal model of the dry hot rock is set as a 100 m × 100 m two-dimensional square heat extraction area, with two fractures in the model. The horizontal fracture has a length of 100 m, and the vertical fracture has a length of 15 m. The width of the fracture is denoted by dz. In Figure 1, the blue point a represents the injection well, and the red point c represents the production well. The coordinates of injection well a are 0 and 50, and the coordinates of production well c are 50 and 25. The model correlation parameters are shown in Table 1.

2.4.2. Boundary Condition. The initial and boundary conditions are specified as follows:

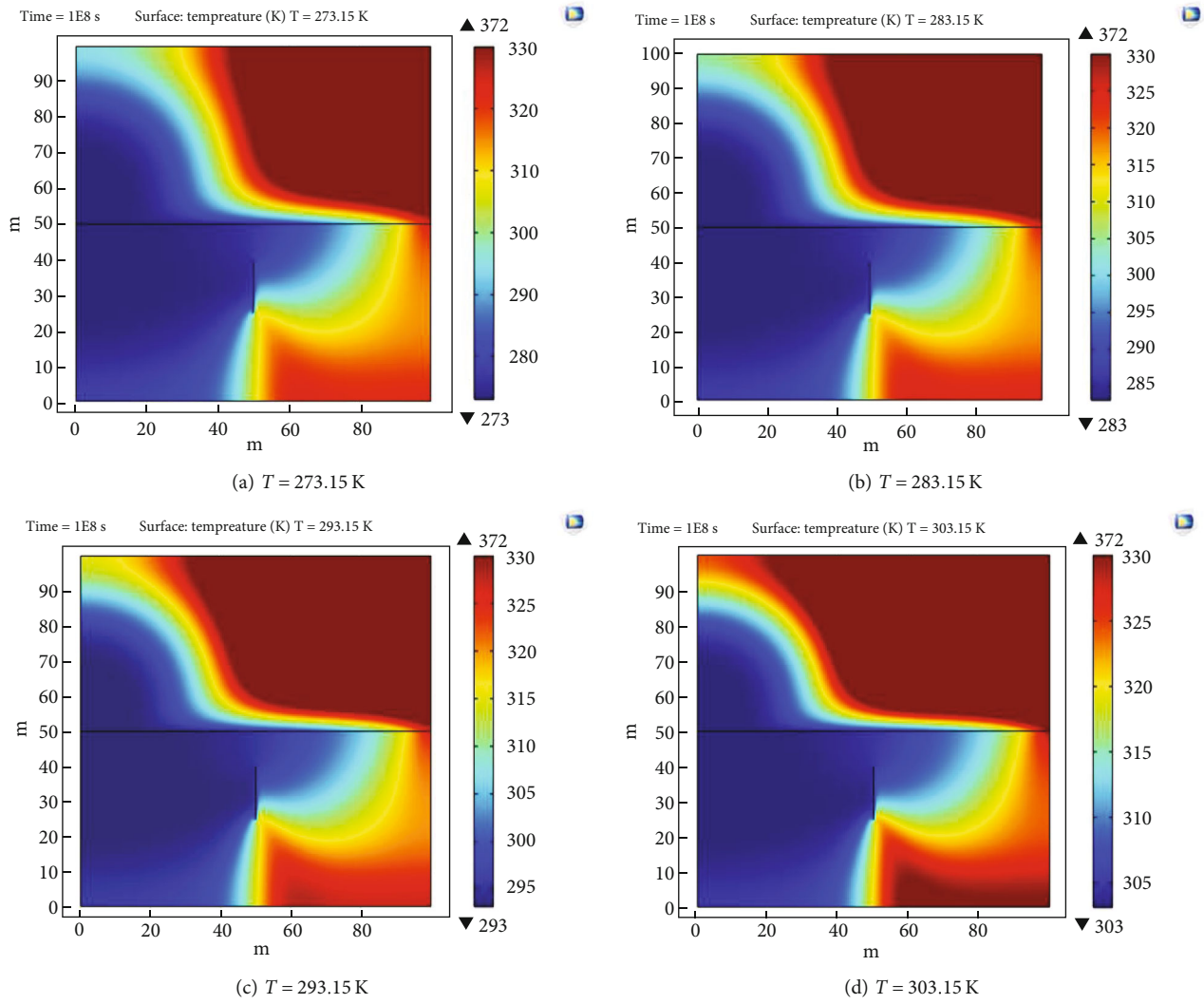

(a) $T = 273.15$ K (b) $T = 283.15$ K

(c) $T = 293.15$ K (d) $T = 303.15$ K

Figure 6: Temperature field cloud image of fractured rock mass at different injection temperatures ($t = 10^8$ s).

In this model, the upper and lower boundaries of the fractures are defined as impermeable boundaries. The left boundary is designated as the inflow boundary for the low-temperature medium, while the outflow boundary for the heat-extracting medium is located at the extraction well. Before the injection of the low-temperature fluid, the initial water pressure within the reservoir is set at 20 MPa. The injection well has a pressure of 40 MPa, and the production well has a pressure of 10 MPa.

The reservoir is initially at a temperature of 373.15 K (100°C), while the injected well water has a temperature of 293.15 K (20°C). The boundaries on both sides of the rock mass are taken as adiabatic boundaries.

In the simulation of the stress field, the surrounding boundaries are set as displacement-constrained boundaries, and the initial stress of the ground is not considered.

2.4.3. Mesh Partitioning. The COMSOL numerical simulation software has the capability of automatic mesh generation. For the rock matrix, a tetrahedral mesh is used, while a triangular mesh is used for the fractures. Figure 2 displays the schematic diagram illustrating the mesh partitioning.

3. Numerical Analysis of Seepage and Heat Transfer in Fractured Rock Mass

3.1. The Evolution Laws of Temperature Field, Stress Field, and Seepage Field

3.1.1. Temperature Field. Figure 3 displays the contour plot of the temperature field within the fractured rock mass under initial conditions. The figure reveals that during the initial extraction phase, heat exchange occurs between the low-temperature working fluid and the high-temperature rock mass, causing an increase in water temperature. This phenomenon arises due to the higher initial temperature of the rock mass within the reservoir compared to the lower temperature of the injected working fluid in the well. Upon the entry of the low-temperature working fluid into the reservoir, it interacts with and transfers heat from the

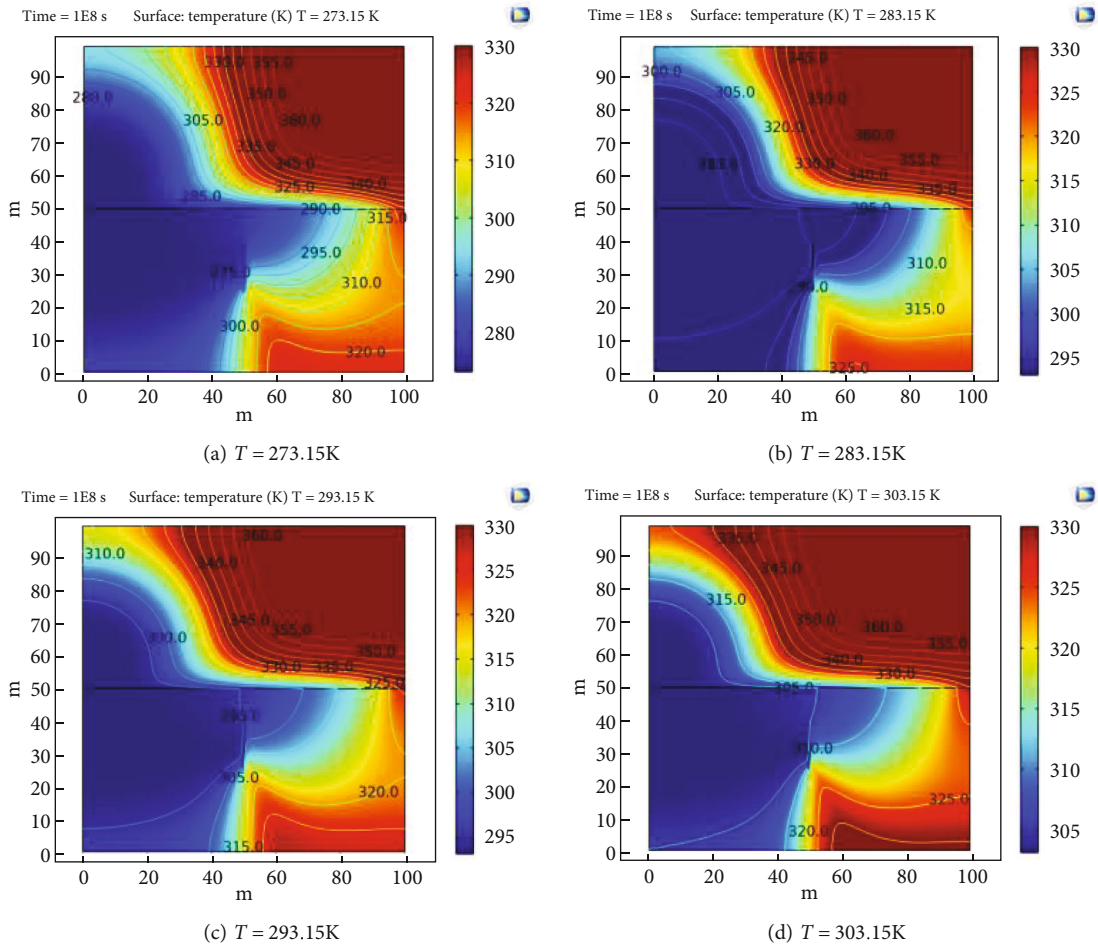

(a) $T = 273.15$K (b) $T = 283.15$K

(c) $T = 293.15$K (d) $T = 303.15$K

Figure 7: Contour plots of the temperature field in the fractured rock mass at various injection temperatures are shown below ($t = 10^8$ s).

high-temperature rock mass, leading to an elevation in the working fluid's temperature and a reduction in the rock mass temperature.

A region of lower temperature emerges in proximity to the injection well and subsequently propagates gradually towards the production well. This is because the vicinity of the injection well is the main area for heat exchange and transfer within the reservoir, and it is where the majority of heat loss occurs. Over time, the temperature of the surrounding rock in the vicinity of the injection well steadily diminishes, creating a low-temperature zone that centers around the injection well and expands outward. This low-temperature zone will spread towards the production well direction with the flow of fluids, affecting a larger area.

The low-temperature zone primarily spreads along fracture surfaces while the diffusion in the matrix rock is slower. This is because fracture surfaces serve as the main pathways and heat transfer mediums for fluids within the reservoir, offering higher flow velocity and heat transfer capacity. Heat exchange and transfer occur more rapidly on fracture surfaces. Thus, the low-temperature zone tends to spread preferentially along fracture surfaces. On the other hand, the matrix rock acts as a secondary pathway and heat transfer medium for fluids within the reservoir, characterized by lower flow velocity and heat transfer capacity. Heat exchange and transfer on the matrix rock occur at a slower pace.

In summary, the temperature distribution within the reservoir gradually transitions from high to low over time, with a discernible low-temperature zone emerging near the injection well. Additionally, during this timeframe, it becomes evident that the low-temperature zone expands more rapidly along fracture surfaces compared to the slower diffusion within the matrix rock.

3.1.2. Stress Field. The stress field cloud map within the fractured rock mass is shown in Figure 4. In Figure 4, it can be observed that the fractured rock mass in the reservoir experiences a temperature decrease due to the extraction of heat by low-temperature water. As the rock mass temperature decreases, the rock contracts, which impacts the stress field of the matrix. This is because the rock deformation and displacement are caused by the temperature decrease. Furthermore, the reduction in rock mass temperature induces alterations in various physical properties of the rock, including density, elastic modulus, and Poisson's ratio.

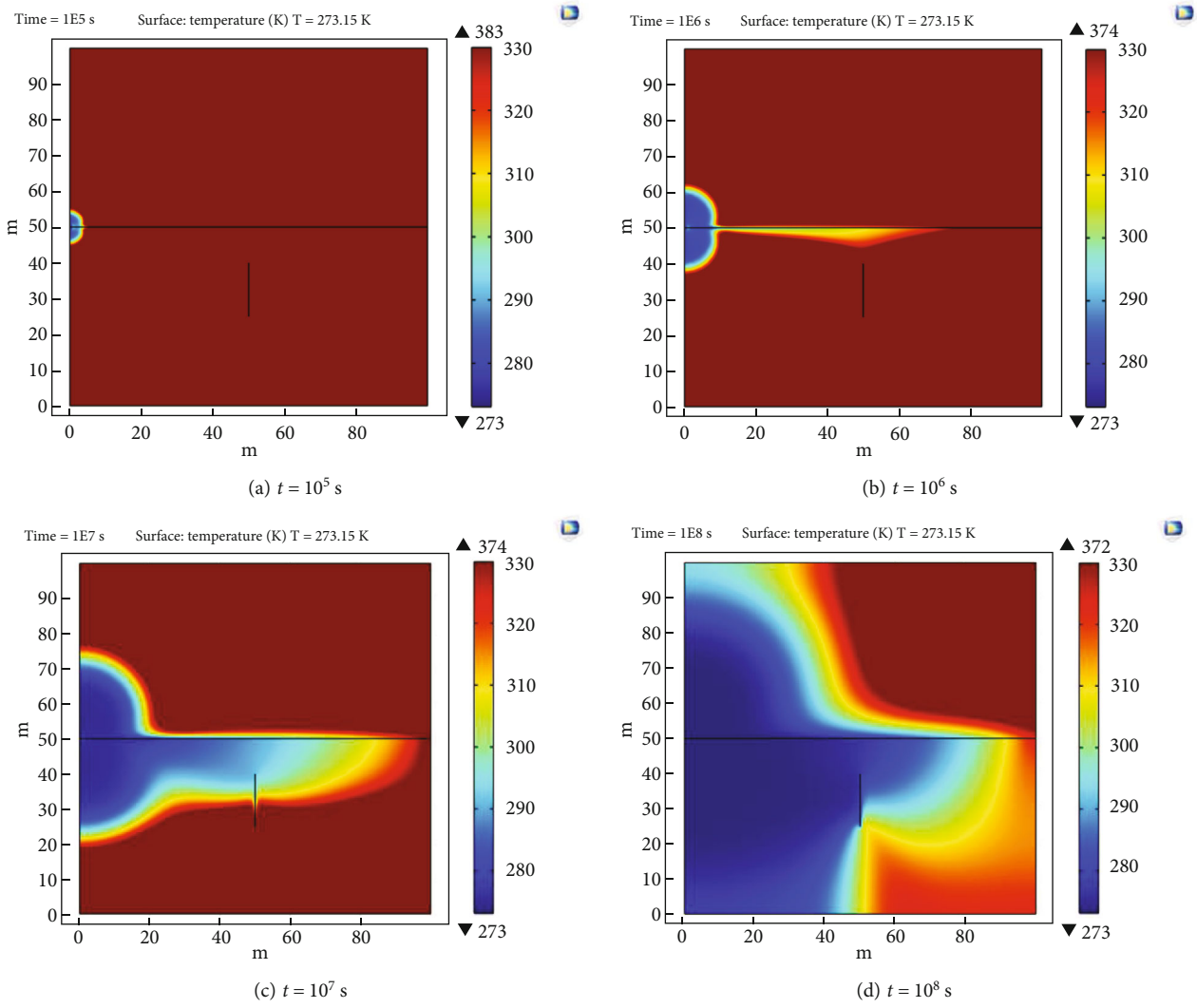

Figure 8: Temperature cloud image when injection temperature is 0°C.

These changes influence the stress state of the rock mass, especially the matrix stress field. The matrix stress field represents the stress distribution acting on the reservoir rock mass matrix, providing insight into the strength and stability of the rock mass.

Rock contraction alters the opening of rock fractures. Over time, the fracture aperture widens, resulting in enhanced permeability and improved heat transfer efficiency. This is because the larger fracture aperture increases the fluid flow velocity and heat transfer capacity within the fractures, enabling more thorough heat exchange and transfer. The increased fracture aperture leads to higher fluid pressure within the fractures, exerting greater pressure on the rock mass. Moreover, the flow along the fracture surfaces intensifies, allowing water to reach the production well more quickly. The flow advantage becomes more prominent, causing an imbalance in heat transfer between the fracture zone and the surrounding area. Consequently, this leads to changes in thermal stress and variations in the stress field.

The stress within the reservoir increases over time, similar to the temperature field distribution. This is because the stress within the reservoir is determined by the thermal stress and fluid pressure inside the reservoir. With the passage of time, variations arise in the temperature and pressure within the reservoir, subsequently impacting thermal stress and fluid pressure, thereby influencing the stress state within the reservoir. Generally, the reservoir experiences a gradual distribution of temperature and pressure, characterized by a gradient from high to low, similar to the temperature field distribution.

3.1.3. Seepage Field. Figure 5 shows the permeability field cloud map of the fractured rock mass. From the figure, it can be observed that the fluid flow velocity within the fractures varies with time. The high-velocity region initially expands and then contracts. This is because the fluid flow velocity within the fractures is influenced by the pressure and temperature differences within the fractures. With the passage of time, changes occur in the pressure and

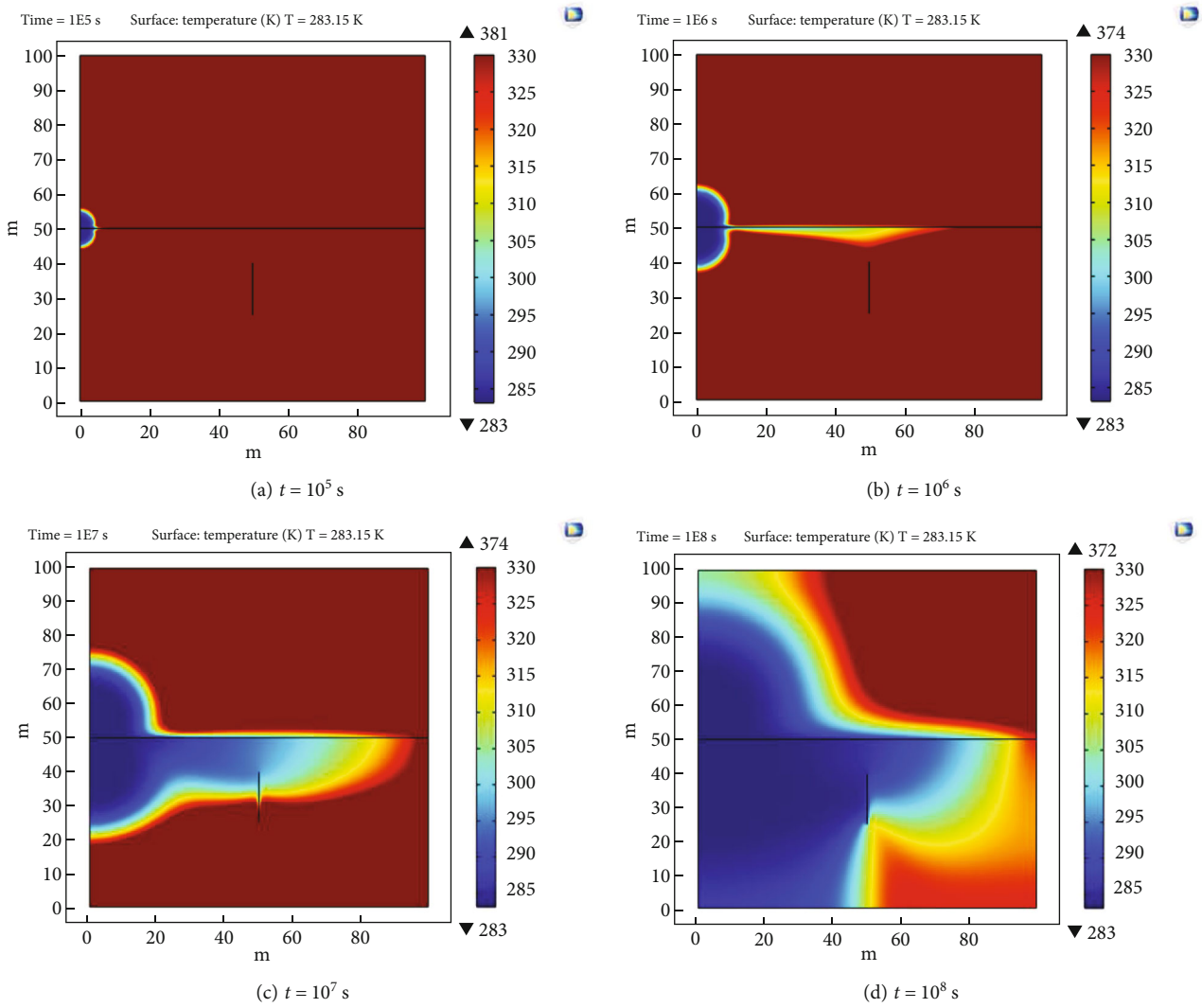

Figure 9: Temperature cloud image when injection temperature is 10°C.

temperature differences within the fractures, resulting in variations in the fluid flow velocity within the fractures. Typically, in the initial phase of extraction, the pressure and temperature disparities within fractures are greater, leading to higher fluid flow velocities and larger high-velocity regions. As extraction progresses into the intermediate and later stages, the pressure and temperature differences within fractures diminish, resulting in lower fluid flow velocities and smaller high-velocity regions.

The streamlines at the two wells are dense, while the flow is weak or absent in the edge regions. This is because the two wells serve as the inlet and outlet of the fluid within the reservoir, representing the main flow direction of the fluid within the reservoir. Therefore, the fluid flow velocities are higher and the streamlines are denser at the two wells. The edge regions, on the other hand, are far from the injection and production wells and represent ineffective regions for fluid flow within the reservoir.

The dominant flow regions have a higher heat extraction capacity, while the disadvantaged flow regions have a lower heat extraction capacity. This is because the dominant flow regions refer to the main active areas of fluid flow within the reservoir, where heat exchange and transfer occur predominantly. Hence, the dominant flow regions have a higher heat extraction capacity, allowing the heat energy within the reservoir to be extracted more quickly and resulting in a faster decrease in reservoir temperature. The disadvantaged flow regions, on the other hand, represent secondary active or ineffective areas for fluid flow within the reservoir, where heat exchange and transfer occur to a lesser extent or not at all. Therefore, the disadvantaged flow regions have a lower heat extraction capacity, leading to a slower extraction of heat energy from the reservoir or no change in reservoir temperature.

3.2. The Influence of Injection Water Temperature on Heat Recovery

3.2.1. The Impact of Injection Water Temperature on the Temperature Distribution. The variation pattern of the

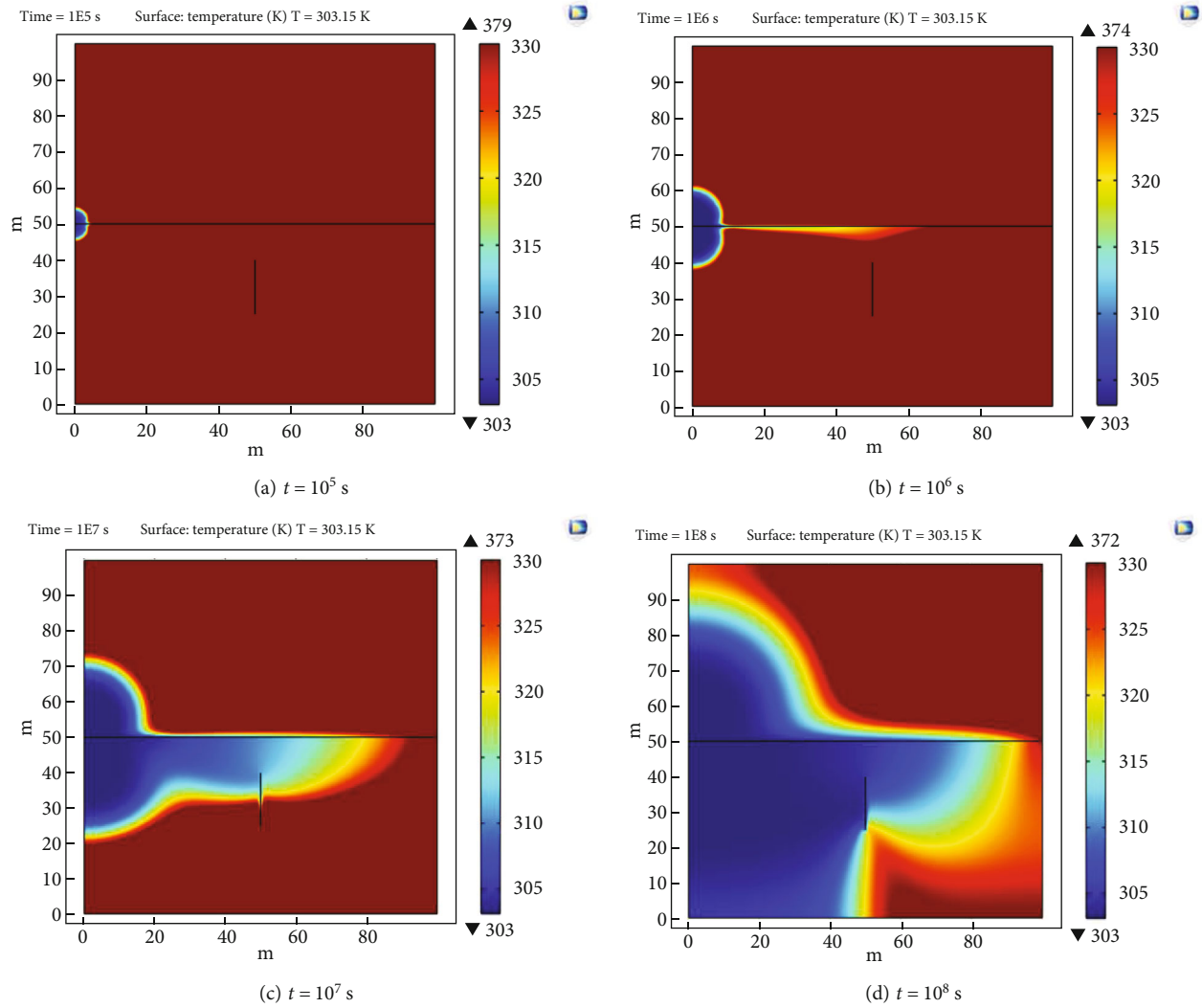

Figure 10: Temperature cloud image when injection temperature is 30°C.

temperature field with injection water temperatures is set at 273.15 K (0°C), 283.15 K (10°C), 293.15 K (20°C), and 303.15 K (30°C), respectively. The temperature field cloud diagrams for the fractured rock mass under four different injection water temperatures are shown in Figure 6.

Based on Figure 6, the general features of the rock mass temperature field remain consistent regardless of the injection temperatures. However, an increase in injection water temperature leads to a corresponding rise in the average rock mass temperature.

Based on Figure 7(a), it can be observed that along the flow direction, the contour lines of the rock mass temperature become sparser. This is because, along the flow direction, the water velocity and heat transfer capacity within the rock mass are higher, leading to faster heat exchange and transfer. As a result, the temperature distribution within the rock mass becomes more uneven, and the temperature variation becomes larger along the flow direction, resulting in sparser contour lines. Similarly, increasing the injection water temperature will also lead to sparser contour lines in the rock mass temperature field. Reducing the injection water temperature enhances the heat exchange rate, expands the low-temperature zone, and diminishes the reservoir's lifespan. This is due to the increased temperature disparity between the reservoir water and rock mass, resulting in accelerated heat exchange and transfer within the reservoir. Consequently, heat is extracted from the reservoir more rapidly, causing the reservoir's temperature to decrease more quickly and expanding the low-temperature zone, ultimately shortening the reservoir's lifespan.

Figures 8–10 show the distribution of temperature fields with respect to production time for injection well water temperatures of 0°C, 10°C, and 30°C, respectively. By comparing these three sets of figures with Figure 3, it can be observed that there is almost no difference in the temperature field distribution during the heat extraction period of 10^5 s-10^6 s. However, as the heat extraction progresses from 10^7 s-10^8 s, the low-temperature area in reservoirs with lower injection water temperatures becomes larger compared to those with higher injection water temperatures. The use of colder injection water also leads to a shorter reservoir lifespan and increases reservoir stress and fractures, resulting in the

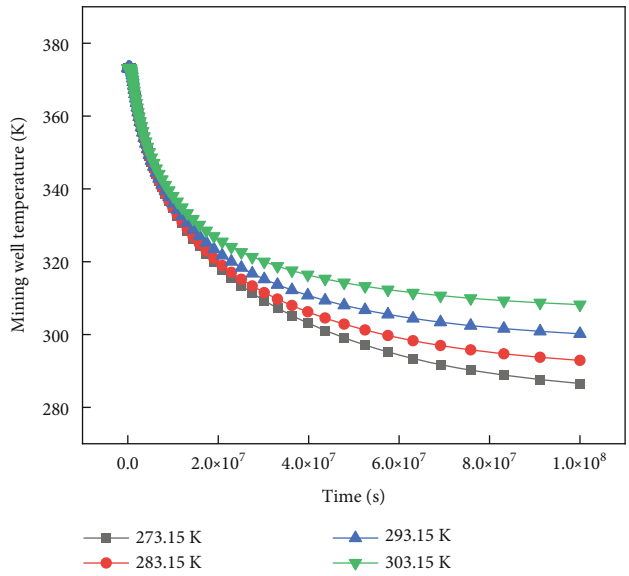

Figure 11: Production well temperature diagram at each injection temperature.

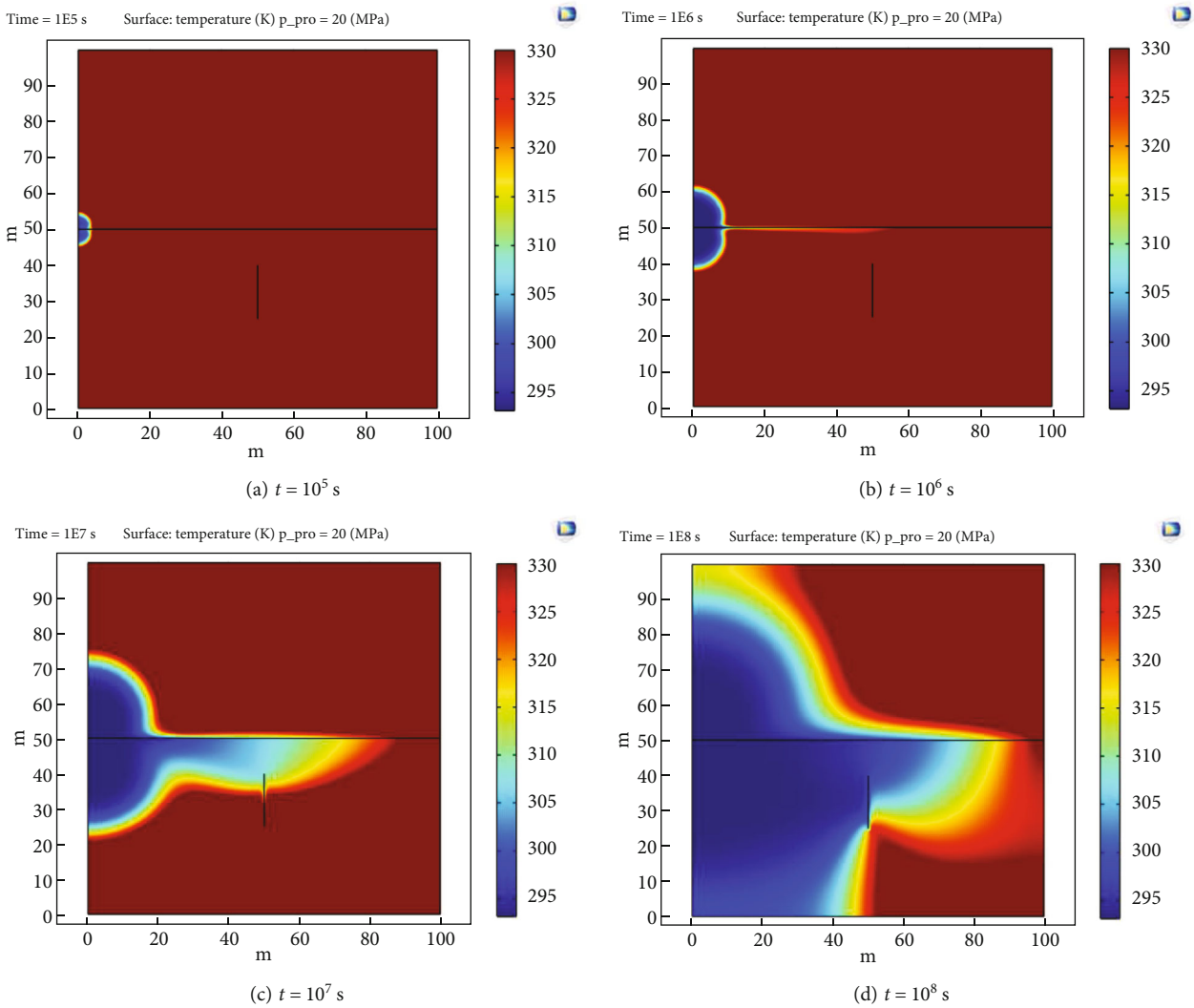

(a) $t = 10^5$ s

(b) $t = 10^6$ s

(c) $t = 10^7$ s

(d) $t = 10^8$ s

Figure 12: Distribution of reservoir temperature field with time when injection and production pressure difference is 20 MPa.

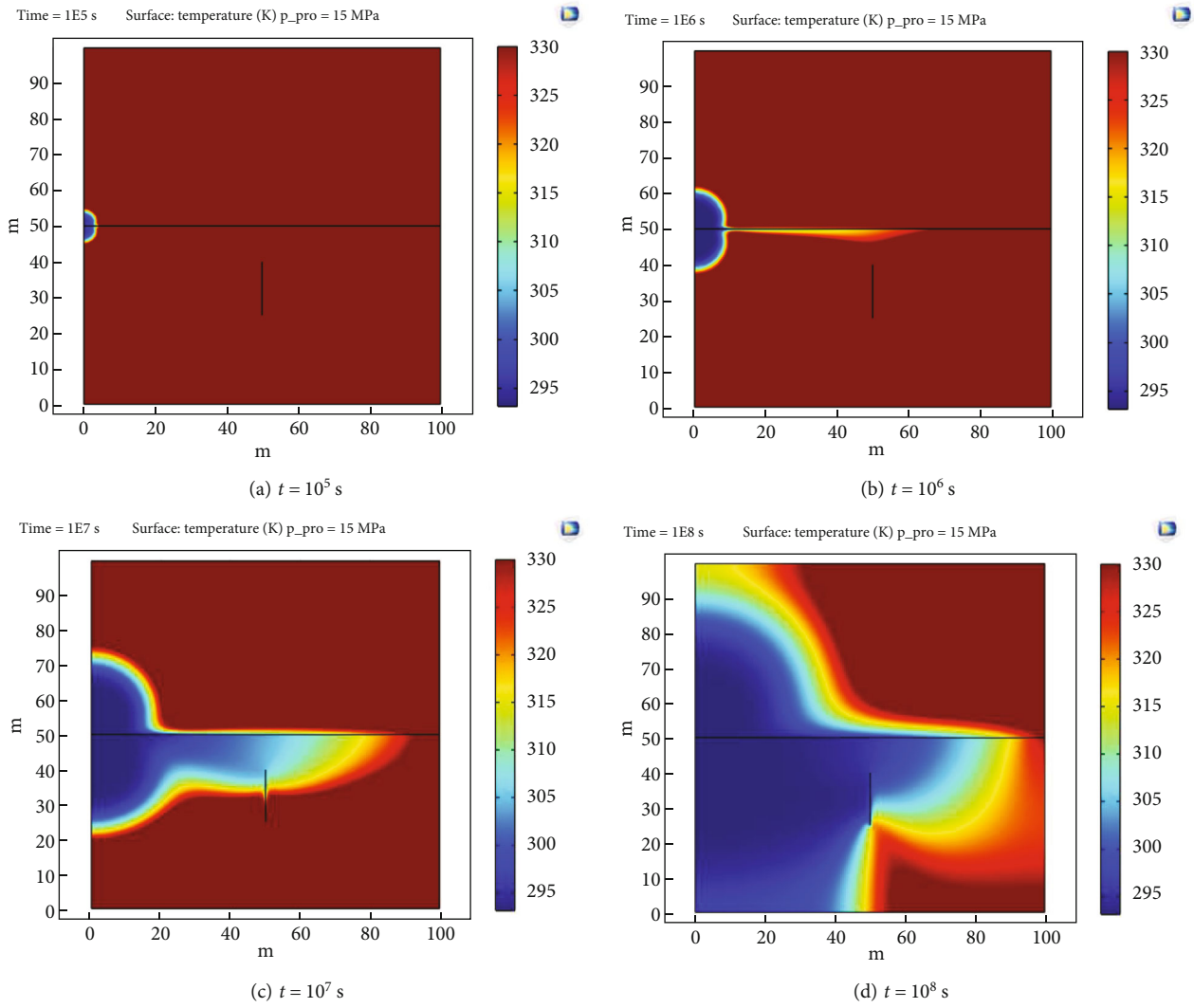

(a) $t = 10^5$ s (b) $t = 10^6$ s

(c) $t = 10^7$ s (d) $t = 10^8$ s

Figure 13: Distribution of reservoir temperature field with time when injection and production pressure difference is 25 MPa.

deterioration of the reservoir's physical and mechanical properties.

Different stages of production require adjustments in the injection water temperature to adapt to reservoir changes and optimize production efficiency. Generally, during the initial stages of production, lower injection water temperatures can be used to reduce injection costs and energy consumption. In the later stages of production, the injection water temperature can be gradually increased to enhance the heat extraction rate. This approach helps balance the production rate and reservoir lifespan, enabling sustainable development of the reservoir. By properly controlling the injection water temperature, premature depletion of the reservoir's energy and resources can be avoided, thereby extending the reservoir's utility life. Moreover, it can increase the economic and societal benefits of hot dry rock reservoirs while reducing environmental pollution and risks.

3.2.2. Effect of Water Injection Temperature on Extraction Well Temperature. According to Figure 11, it can be observed that the higher the temperature of the injected fluid, the shorter the time required for the rock mass temperature field to reach a steady state. High-temperature injection water can accelerate the thermal stabilization of the rock mass. This is because high-temperature water can more rapidly transfer heat to the rock mass, allowing the rock mass temperature to reach a level similar to or close to that of the injected water. The use of high-temperature injection water additionally aids in reducing stress and fractures within the rock mass, thereby improving its strength and stability. The gradual decrease in production well water temperature over time is primarily attributed to the continuous extraction of heat from the reservoir by the production well, resulting in a gradual decline in reservoir temperature. The decrease in the temperature of the production well water also reflects the consumption of energy and depletion of resources in the reservoir.

During the early stage of heat extraction, the temperature of the injected water has a minimal impact on the output temperature. This is because, in the early stage, the heat

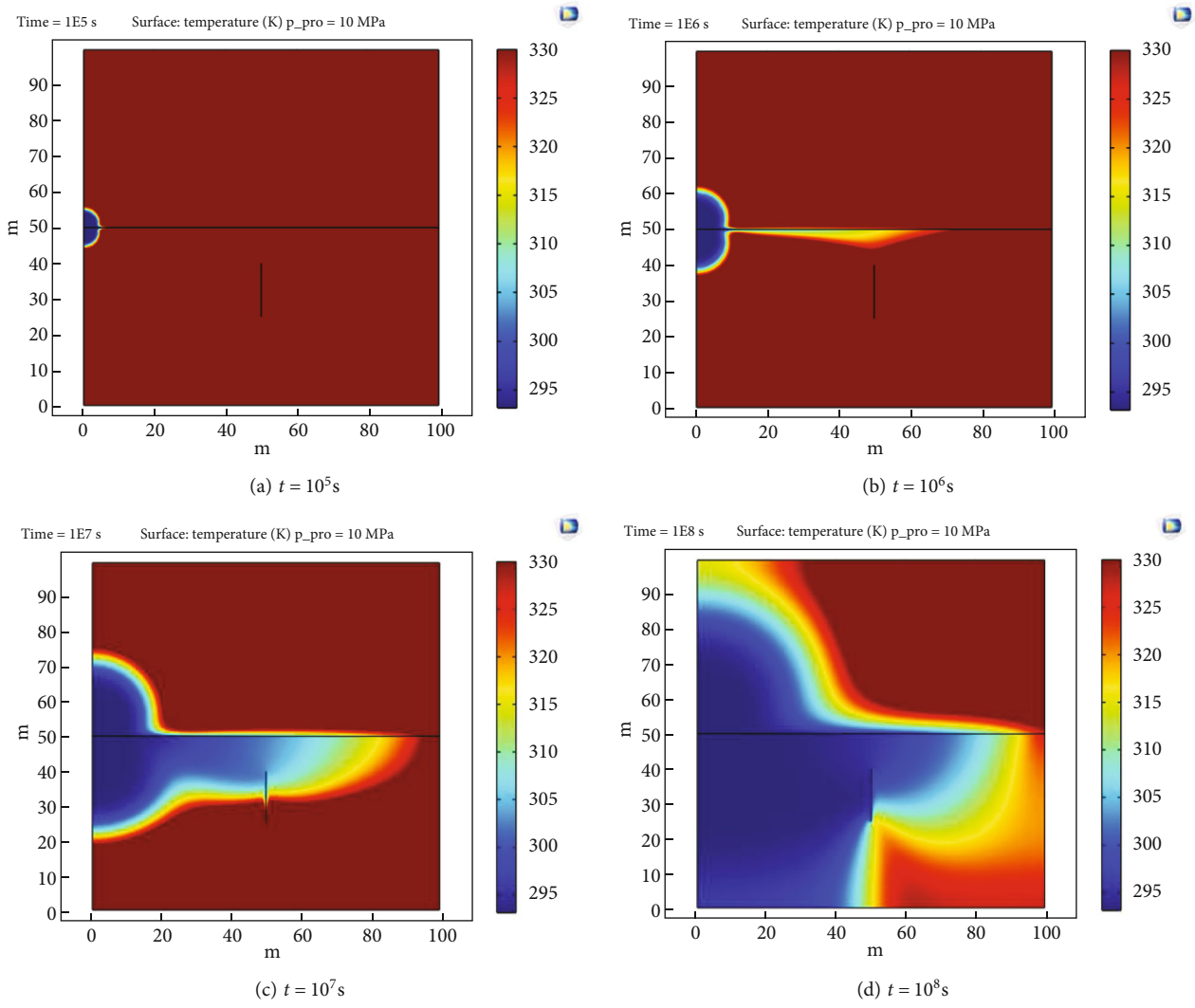

(a) $t = 10^5$s (b) $t = 10^6$s

(c) $t = 10^7$s (d) $t = 10^8$s

Figure 14: Distribution of reservoir temperature field with time when injection and production pressure difference is 30 MPa.

within the reservoir has not been significantly exchanged or extracted yet, and the reservoir temperature remains relatively high. The changes in the injected well water temperature take some time to propagate to the vicinity of the production well. Hence, in the initial phase of heat extraction, the outlet temperature of the production well is predominantly determined by the temperature of the reservoir itself. For example, at the beginning of the operation (4.786×10^5 s), the outlet temperature of all four production wells is 100°C. Yet, in the intermediate to advanced stages of heat extraction, the injected water temperature plays a substantial role in determining the output temperature. This is because, at this stage, a substantial amount of heat has already been extracted from the reservoir, causing the reservoir temperature to decrease. Fluctuations in the temperature of the injected well water can expediently influence the temperature in the vicinity of the production well. Hence, in the intermediate to advanced stages of heat extraction, the outlet temperature of the production well is predominantly influenced by the temperature of the injected well water. Increasing the injected water temperature can extend the lifespan of the reservoir because it improves the recovery efficiency of heat within the reservoir.

3.3. Influence of Injection and Extraction Differential Pressure on Heat Extraction

3.3.1. Influence of Injection and Mining Differential Pressure on the Temperature Field. The effect of the injection-production pressure difference on the reservoir temperature field is illustrated in Figures 12–15. By examining four different scenarios (with a constant injection pressure of 40 MPa and varying production pressures of 5 MPa, 10 MPa, 15 MPa, and 20 MPa), we analyze the impact and mechanism of different injection-production pressure differences on the reservoir's temperature field.

The pressure difference between injection and production significantly influences fluid velocity and heat transfer within the thermal reservoir. This is due to its role in determining the flow direction, affecting fluid motion and heat

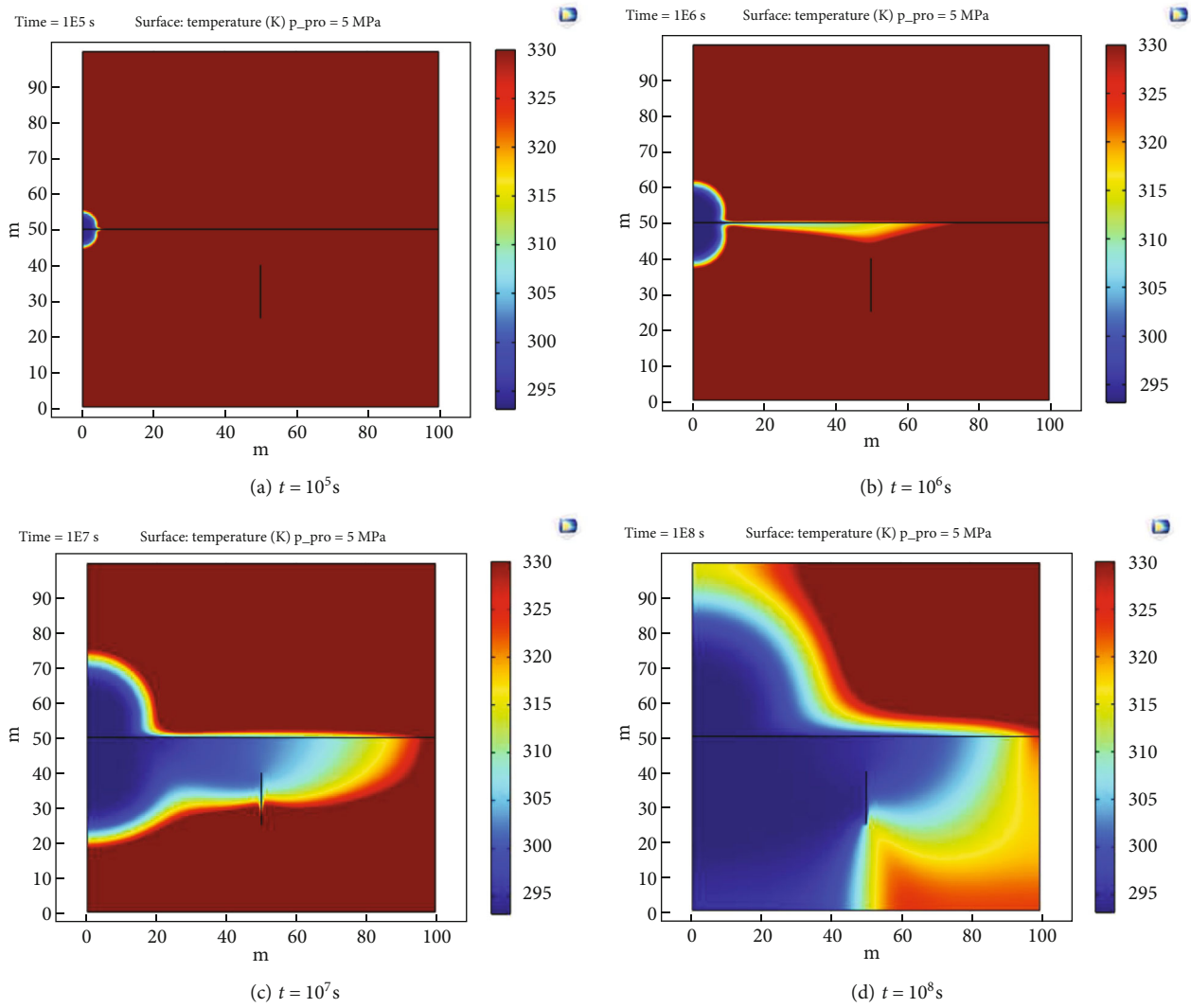

(a) $t = 10^5$s (b) $t = 10^6$s

(c) $t = 10^7$s (d) $t = 10^8$s

Figure 15: Distribution of reservoir temperature field with time when injection and production pressure difference is 5 MPa.

distribution. A larger pressure difference results in higher fluid velocity and heat transfer capability, leading to faster heat exchange within the reservoir. As the injection-production pressure difference increases, the heat extraction rate and expansion of the low-temperature zone within the reservoir also increase. This is because a larger injection-production pressure difference leads to higher fluid velocity and heat transfer capability, resulting in faster extraction of heat from the reservoir and thus a faster decrease in reservoir temperature. As the extraction time extends, the low-temperature zone gradually extends towards the direction of the injection well, forming a temperature gradient. However, an excessively large injection-production pressure difference can also affect the heat extraction efficiency of the reservoir. This is because an excessively large pressure difference results in excessively high fluid velocity and heat transfer capability within the reservoir, leading to rapid depletion of heat from the reservoir and a rapid decrease in reservoir temperature. This will waste energy, cause resource loss, and reduce the heat extraction efficiency and economic benefits of the reservoir.

The injection-production pressure difference should be carefully balanced to ensure a sustainable and efficient use of the reservoir, considering factors such as heat extraction rate, capability, efficiency, and lifespan. This approach is aimed at achieving optimal utilization and long-term development of the reservoir. The setting of the injection-production pressure difference should be reasonably selected and adjusted based on the characteristics of the reservoir, extraction goals, technical conditions, and other factors to achieve the best heat extraction efficiency and lifespan.

3.3.2. The Impact of Injection Pressure Difference on the Temperature of Extraction Wells. Figure 16 displays the production temperature variation at the production well for different injection-production pressure differences of 20 MPa, 25 MPa, 30 MPa, and 35 MPa.

During the initial 3.981×10^5 seconds of heat extraction, the temperature at the production well is consistently 100°C, and then it starts to decrease. After 1×10^7 seconds of heat extraction, the temperatures at the production well are 70.46°C, 66.25°C, 62.77°C, and 60.29°C, with decreases of

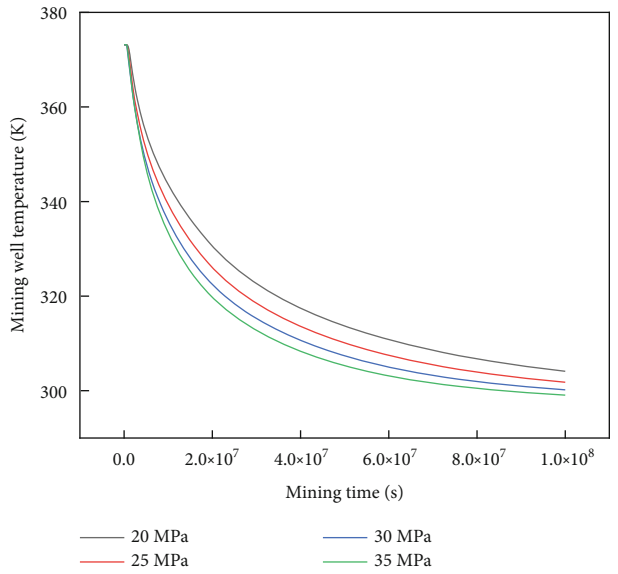

Figure 16: Temperature diagram of mining well under different pressure differences.

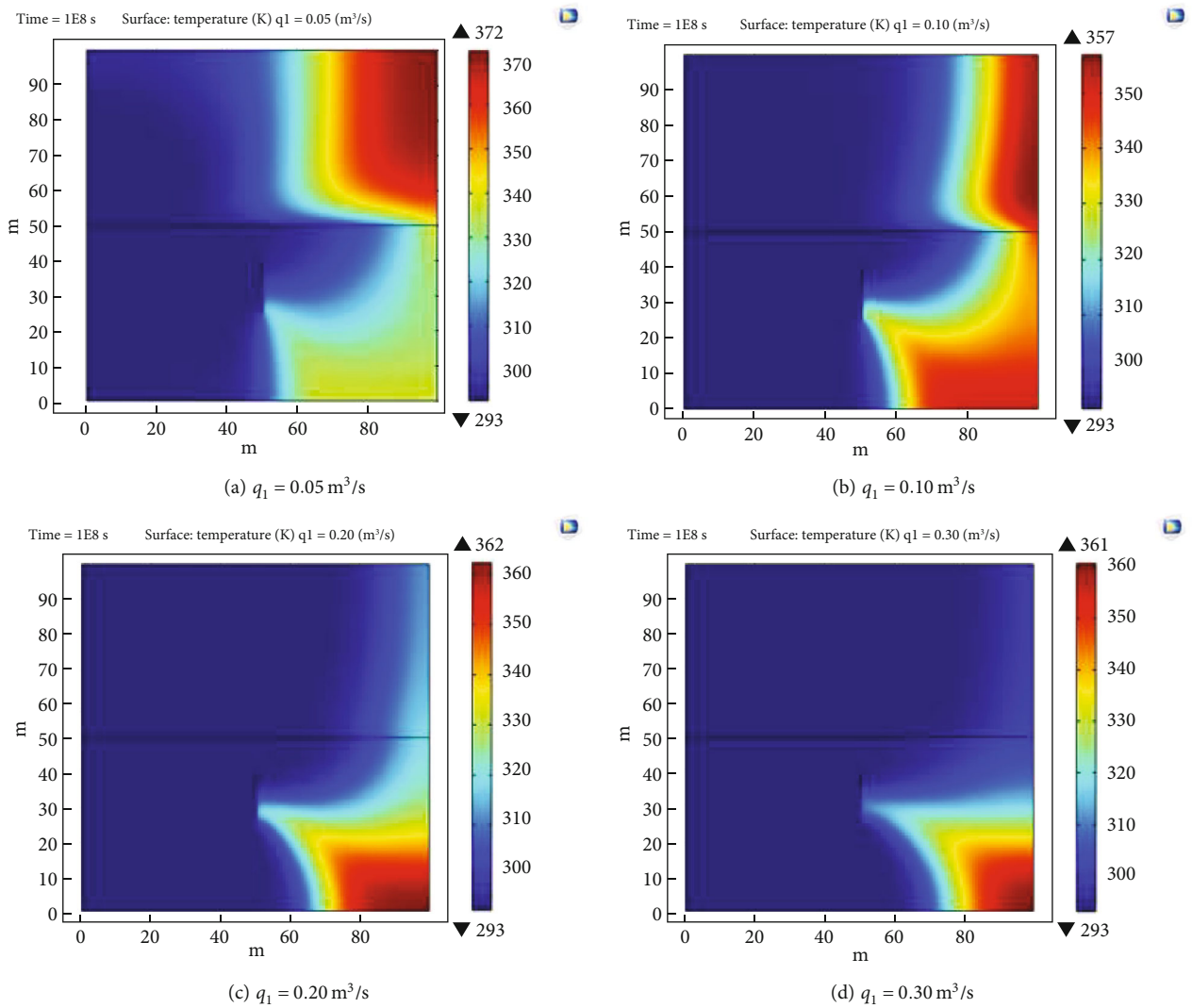

Figure 17: Temperature field cloud image under different flow rates at the same time ($t = 10^8$ s).

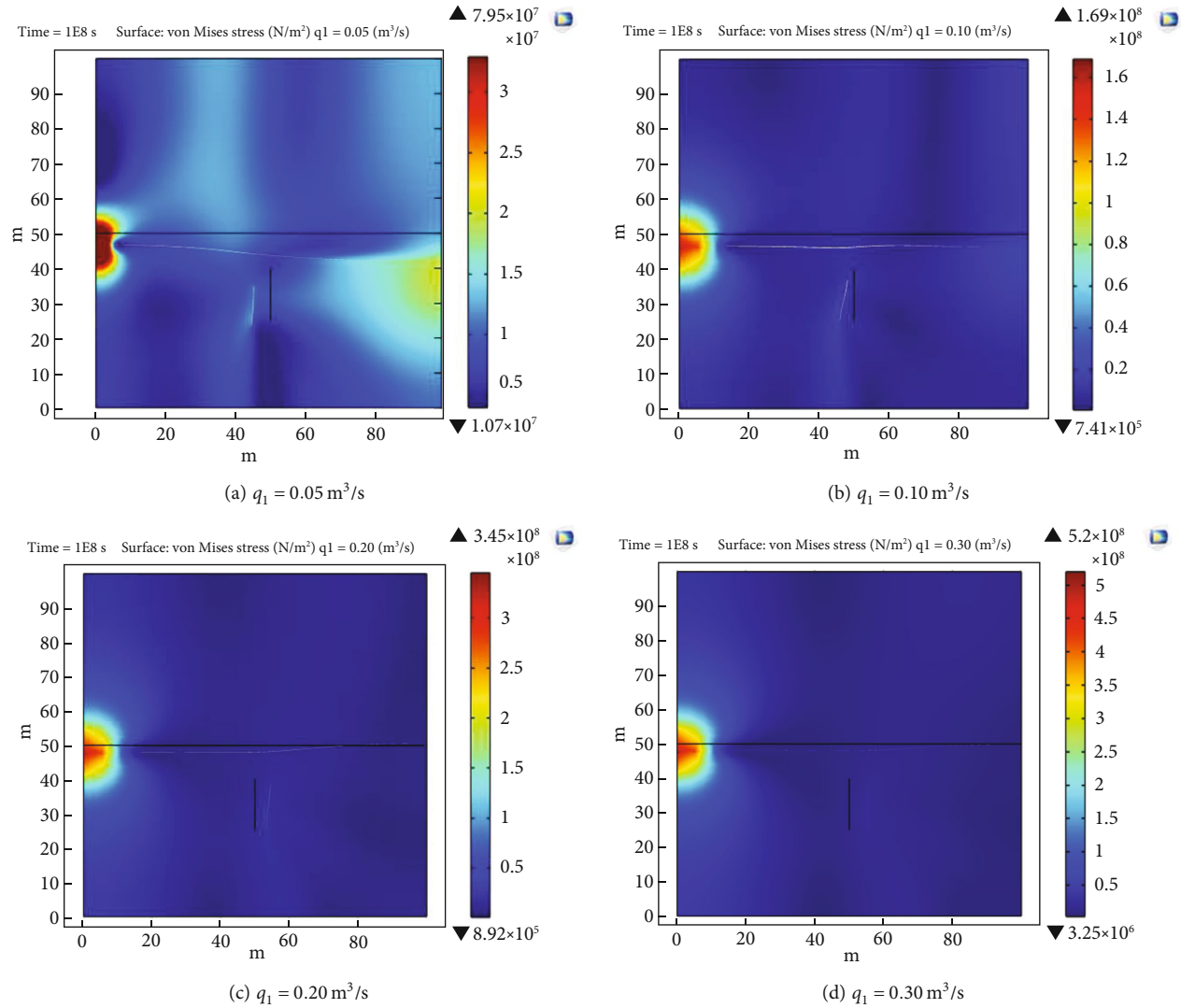

(a) $q_1 = 0.05\ m^3/s$ (b) $q_1 = 0.10\ m^3/s$

(c) $q_1 = 0.20\ m^3/s$ (d) $q_1 = 0.30\ m^3/s$

FIGURE 18: Cloud map of stress field under different flow at the same time ($t = 10^8$ s).

29.54%, 33.75%, 36.23%, and 39.71%, respectively. After 1 $\times 10^8$ seconds of heat extraction, the output temperatures are 30.97°C, 28.63°C, 27.03°C, and 25.91°C, with decreases of 69.03%, 71.37%, 72.97%, and 74.09%, respectively. The larger the pressure difference, the lower the production temperature. Although increasing the pressure difference can enhance the rate of heat generation, it also accelerates the flow velocity of the injected water, causing the water flow to preferentially follow more favorable pathways. This accelerates the decrease in reservoir temperature and leads to an imbalance in the heat extraction rate between the fracture surfaces and the edge regions of the rock mass. As a result, there may still be a significant amount of heat at the reservoir edges that cannot be fully utilized, resulting in a tremendous waste of resources.

3.4. Effect of Injection Flow Rate on Heat Extraction

3.4.1. Effect of Injection Flow Rate on Temperature Field. The EGS system was numerically simulated with injection flow rates of 0.05 m^3/s, 0.10 m^3/s, 0.20 m^3/s, and 0.30 m^3/s while keeping other parameters consistent. Figure 17 shows the temperature distribution contour maps under different injection flow rates. From the figure, it can be observed that with higher injection flow rates, the disturbed area of the rock mass temperature field becomes larger, resulting in a larger low-temperature zone. This is because higher injection flow rates lead to higher fluid velocities and heat transfer capabilities within the rock mass, resulting in faster heat exchange and transfer. As a result, the temperature distribution within the rock mass undergoes changes, leading to the formation of an expanding low-temperature zone centered around the injection well. With an increase in the injection flow rate, both the extent and intensity of the low-temperature zone broaden.

Moreover, with an increase in the injection flow rate, the average temperature of the rock system decreases. This occurs because higher injection flow rates cause increased heat dissipation within the rock system, resulting in a reduction in the overall energy of the rock system. The average

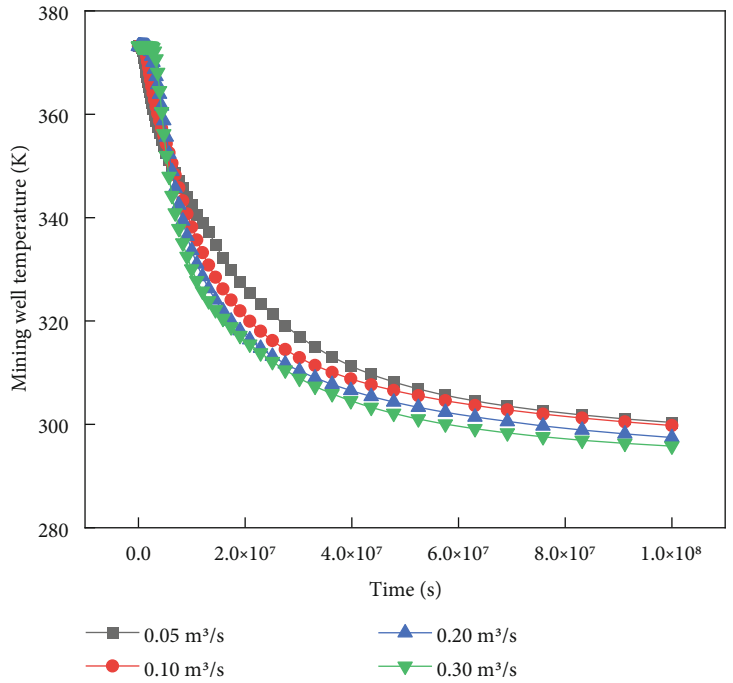

Figure 19: Temperature diagram of production well under each injection flow rate.

temperature of the rock system represents the mean temperature across all points within the rock system and is directly correlated with the total energy of the rock system.

3.4.2. Effect of Injection Flow Rate on the Stress Field. Variations in injection flow rate also impact the stress field distribution within the reservoir. The Cloud map of the stress field under different flows at the same time is shown in Figure 18. Higher injection flow rates correspond to increased stress levels in the rock formation. This is because a higher injection flow rate leads to increased pressure and velocity of the fluid in the rock, exerting larger forces and shear stresses on the rock, thereby altering the stress state and elevating stress levels within the rock. Furthermore, an elevated injection flow rate accelerates temperature fluctuations in the rock, consequently causing heightened thermal stresses within the rock. These combined factors collectively contribute to alterations in the distribution of stress within the rock mass.

Excessive stress in the rock formation increases the risk of dynamic hazards. High-stress levels reduce the strength and stability of the rock, making it more prone to fracturing, sliding, collapsing, and other dynamic phenomena, resulting in damage and failure of the rock mass. These dynamic hazards not only affect the efficiency and lifespan of the enhanced geothermal systems (EGS) but also pose risks to personnel and equipment safety.

Therefore, the selection of injection flow rate should consider the operational reliability of the EGS system to ensure long-term stability and safe operation, while avoiding dynamic hazards and accidents caused by excessively high injection flow rates. The choice of injection flow rate should be determined and adjusted appropriately based on the characteristics, objectives, and conditions of the EGS system, aiming to maintain stress levels within a suitable range in the rock formation.

3.4.3. Impact of Injection Flow Rate on Mining Well Temperature. Figure 19 illustrates the temporal change in well temperature under different injection flow rates. The injection flow rate plays a crucial role in determining fluid dynamics and heat dispersion within the reservoir, thereby influencing heat exchange and transfer. An increased injection flow rate corresponds to higher fluid velocity and enhanced heat transfer capacity within the reservoir, resulting in amplified heat dissipation.

With a larger flow rate, more heat is extracted from the reservoir, causing the temperature to decrease more rapidly. As the production time extends, the temperature within the reservoir gradually approaches a steady level. A higher flow rate corresponds to a lower steady-state temperature. Additionally, a larger flow rate leads to a shorter system lifespan because more energy and resources within the reservoir are consumed at a faster rate, reducing the reservoir's recoverability and economic efficiency.

As time progresses, the temperature of the production well gradually decreases, and a higher injection flow rate accelerates this decline. This is attributed to the fact that the temperature of the production well reflects the extent of heat loss within the reservoir. A higher flow rate corresponds to increased fluid velocity and enhanced heat transfer capacity within the reservoir, leading to a more rapid decrease in temperature. In the initial 5.2481×10^5 seconds (approximately 6 days) of production, the production well temperature remains at 373.15 K. From the 7th day onwards, under the condition of an injection flow rate of 0.05 m^3/s, the

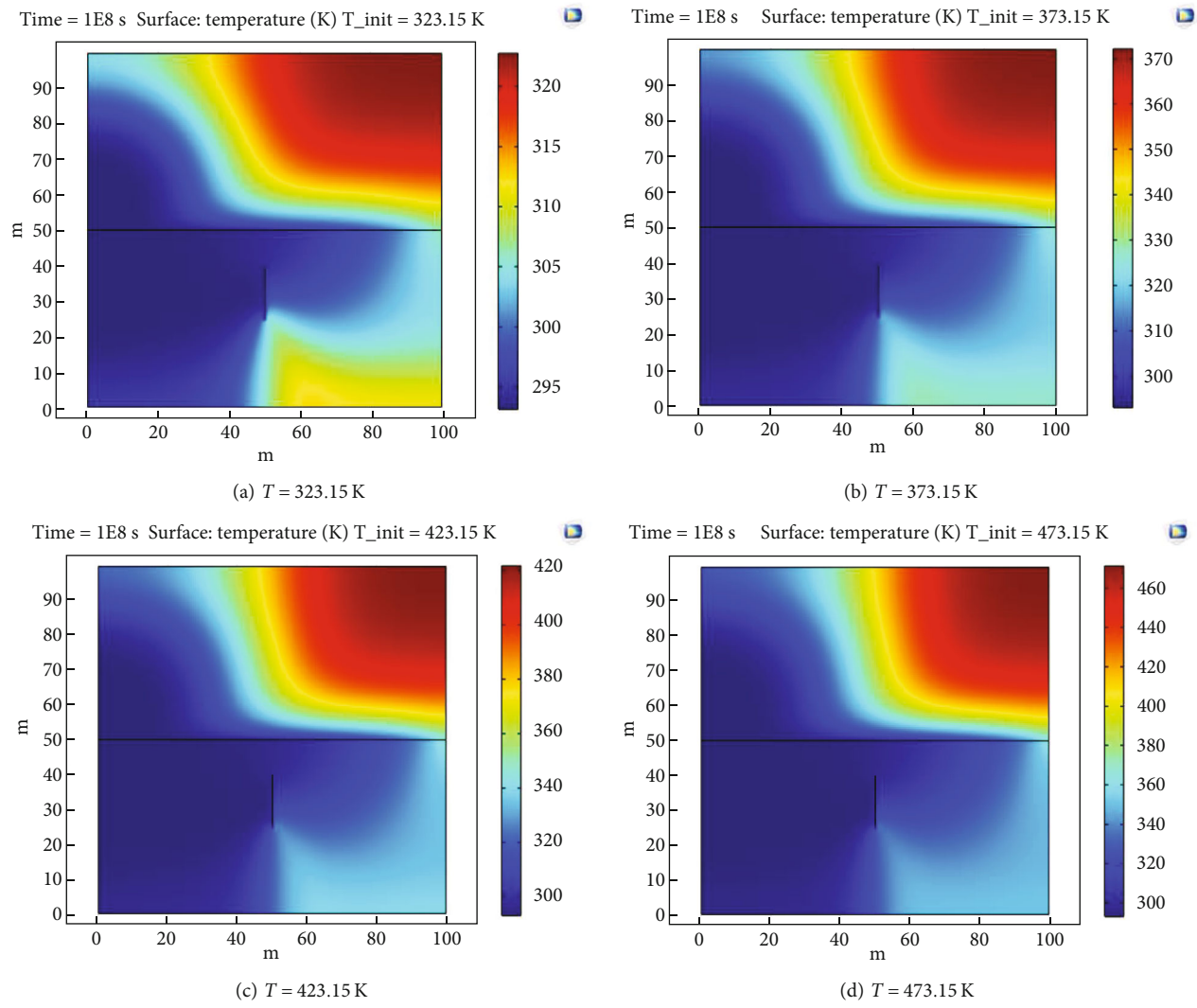

(a) $T = 323.15$ K (b) $T = 373.15$ K

(c) $T = 423.15$ K (d) $T = 473.15$ K

Figure 20: Temperature field cloud image under different initial reservoir temperature at the same time ($t = 10^8$ s).

production temperature starts to decrease significantly. By 1×10^7 seconds (approximately 4 months), the production temperature reaches 69.23°C, representing a decrease of 30.77%. For an injection flow rate of 0.10 m^3/s, the temperature begins to decline from the 10th day. In the case of an injection flow rate of 0.30 m^3/s, the production well temperature only starts to drop after 26 days, and the decline is the fastest, with an average monthly cooling of only 2.59°C.

3.5. Influence of Initial Reservoir Temperature on Heat Recovery

3.5.1. Impact of Initial Reservoir Temperature on the Temperature Field. The temperature field changes after the alteration of initial temperature in different reservoirs can be seen in Figure 20. The temperature variation over time for the same reservoir with an initial temperature of 200°C is illustrated in Figure 21.

Convection heat transfer is achieved by uniformly mixing the water with a temperature difference in the reservoir. Therefore, as the reservoir temperature increases, the temperature difference becomes larger. With a higher temperature difference, water exhibits greater average kinetic energy and requires more energy for collision, resulting in stronger fluidity within the reservoir. Consequently, the diffusion rate of convection is faster, leading to higher heat transfer efficiency and the generation of larger low-temperature regions.

A higher initial reservoir temperature indicates better thermal production performance, with faster heat exchange and transfer within the reservoir. However, this also means that the heat within the reservoir is extracted more rapidly, leading to a faster decrease in reservoir temperature and a shortened lifespan of the reservoir.

In the initial phase of thermal production, the cooling region expands outward, with the temperature near the injection well experiencing the most rapid decline. As thermal production progresses into the intermediate and later stages, a distinct temperature gradient emerges from the injection well to the production well. The cooling region area continues to increase, and the rate of expansion of the cooling region accelerates. However, after reaching a steady state in the later stage of thermal production, the initial

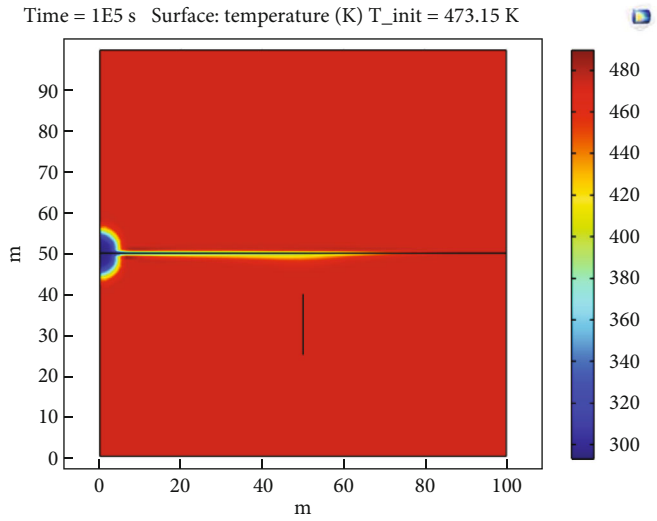

(a) $t = 10^5$s

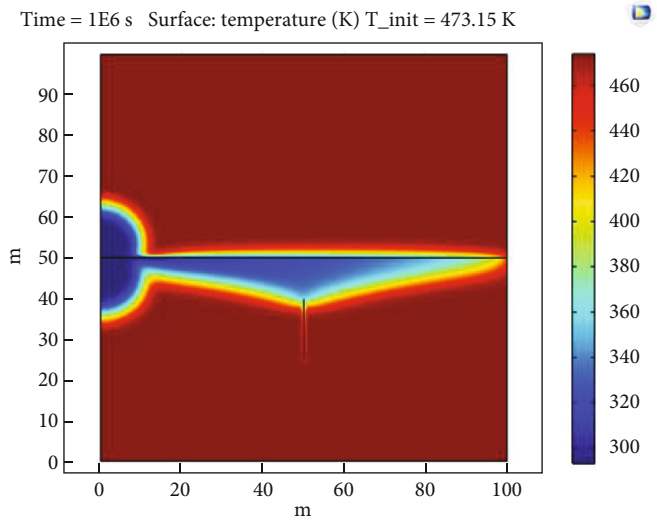

(b) $t = 10^6$s

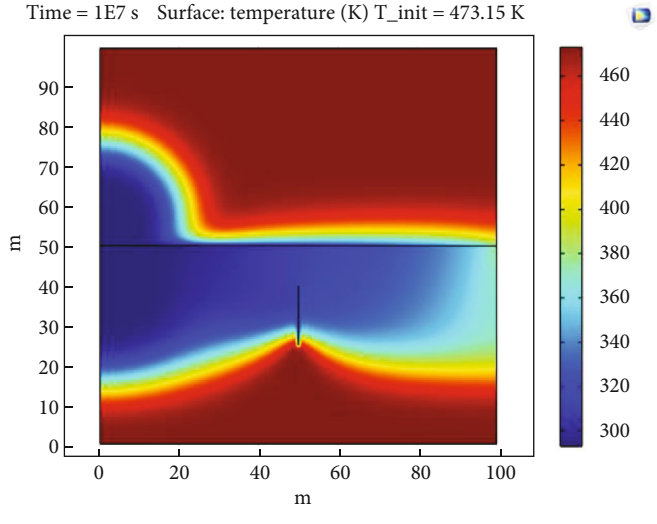

(c) $t = 10^7$s

Figure 21: Continued.

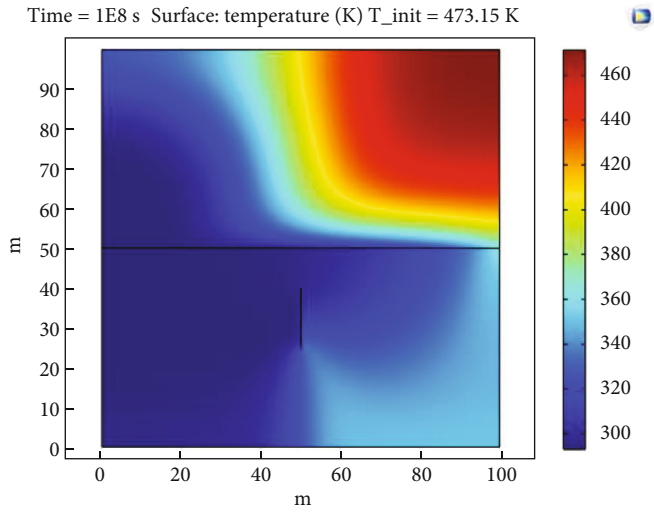

(d) $t = 10^8$s

Figure 21: Temperature field cloud image at different times of the same temperature ($T = 473.15$ K).

temperature has a diminishing impact on the expansion rate of the cooling region. The entire reservoir experiences varying degrees of temperature drop.

The reservoir temperature decreases over time, and the cooling region expands. This is because the reservoir temperature reflects the loss of heat within the reservoir. As time progresses, the heat energy within the reservoir is continuously extracted, leading to a continuous decrease in the reservoir temperature. Simultaneously, the cooling region also spreads outward with time, affecting a larger area.

3.5.2. Effect of Reservoir Temperature on the Stress Field. The stress field variation cloud map can be seen in Figure 22, the maximum principal stress variation pattern in Figure 23, and the enlarged view of the maximum principal stress in Figure 24.

In the initial phase of thermal production, the cooling region expands outward, with the temperature near the injection well experiencing the most rapid decline. As thermal production progresses into the intermediate and later stages, a distinct temperature gradient emerges from the injection well to the production well. During the thermal production process, the maximum principal stress initially decreases and then increases. For example, at 7.9×10^4 seconds after the start of thermal production, the maximum principal stress values corresponding to initial temperatures of 200°C, 150°C, 100°C, and 50°C are 96.4 MPa, 82.4 MPa, 69.84 MPa, and 52.63 MPa, respectively. At 1×10^5 seconds after the start of thermal production, the maximum principal stress values are 88.56 MPa, 71.89 MPa, 61.78 MPa, and 50.57 MPa, respectively. When thermal production reaches 1×10^8 seconds, the maximum principal stress values for the aforementioned initial temperatures are 134.76 MPa, 111.84 MPa, 89.32 MPa, and 67.34 MPa, respectively.

In the early stage of thermal production, the maximum principal stress decreases. This is because, during the initial stage of thermal production, the temperature and pressure changes within the reservoir occur rapidly, resulting in variations in thermal stress and fluid pressure within the rock formation, affecting the stress state of the reservoir rocks. The decrease in the maximum principal stress also leads to a reduction in the strength and stability of the reservoir rocks. In the middle and later stages of thermal production, the maximum principal stress increases. This is because, during the middle and later stages of thermal production, the temperature and pressure changes within the reservoir occur gradually, resulting in variations in thermal stress and fluid pressure within the rock formation, affecting the stress state of the reservoir rocks. The thermal stress weakens while the injection pressure strengthens. With the prolongation of production time, the temperature changes within the reservoir become smaller, leading to a weakening of the thermal stress. Simultaneously, with the prolongation of production time, the temperature and flow rate of the injected well water increase, resulting in enhanced injection pressure.

A higher initial temperature corresponds to increased maximum principal stress and an earlier onset of the upward trend. This is a result of the accelerated heat exchange within the reservoir caused by the higher initial temperature. Consequently, the temperature variations within the reservoir occur at a faster rate, leading to larger fluctuations in thermal stress.

3.5.3. Influence of Reservoir Temperature on Extraction Well Temperature. The temperature variation of the production well at initial temperatures of 200°C, 150°C, 100°C, and 50°C can be seen in Figure 25.

The figure reveals a consistent trend in which the production temperature gradually decreases regardless of the initial temperature. However, it is noteworthy that higher initial temperatures correspond to higher production temperatures. This is because a higher initial temperature results in higher heat storage and output within the reservoir. Additionally, at the same initial temperature, as time progresses, the rate of decrease in production temperature gradually

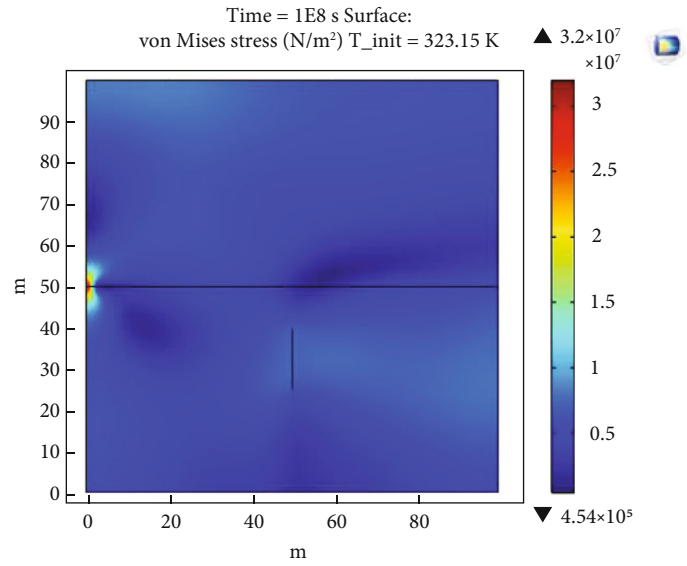

(a) $T = 323.15$ K

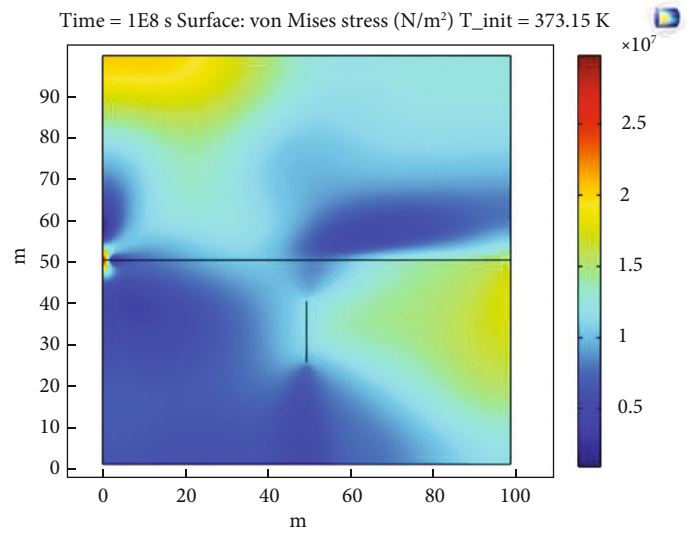

(b) $T = 373.15$ K

Figure 22: Continued.

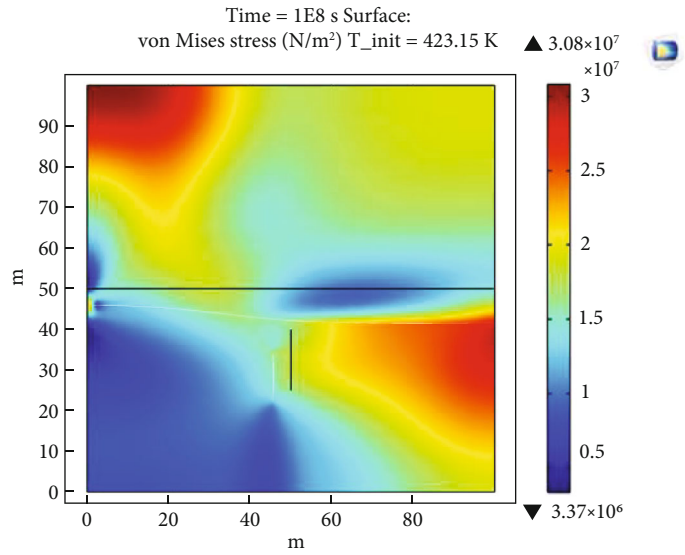

(c) $T = 423.15$ K

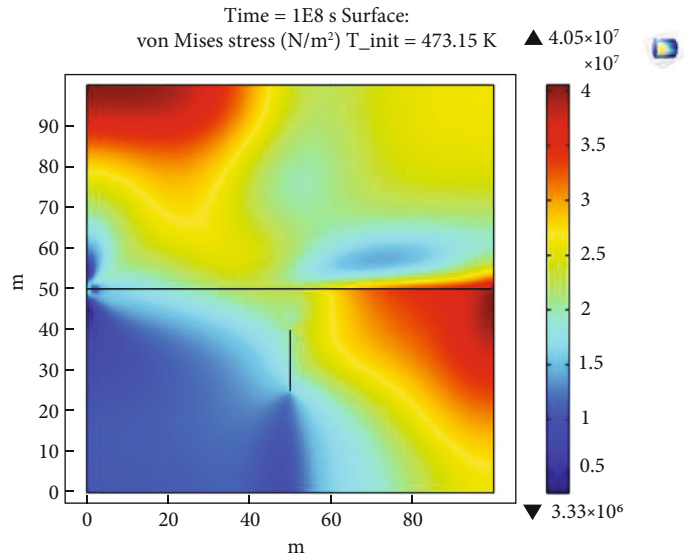

(d) $T = 473.15$ K

Figure 22: Stress nephogram at different initial reservoir temperatures ($t = 10^8$ s).

increases, leading to a continuous decrease in the production temperature. This is because, during the thermal production process, the heat within the reservoir is continuously extracted, causing the temperature of the reservoir to decrease. As the production time extends, the loss of heat and depletion of resources within the reservoir become greater, resulting in a continuous decrease in the production temperature with an accelerated rate of decrease.

Within the first 1.905×10^5 seconds of production, the production temperatures of the well remain at 50°C, 100°C, 150°C, and 200°C, respectively. As the thermal production progresses, the heat transferred from the reservoir to the water becomes smaller than the heat being carried away by the water, leading to a continuous decrease in the production temperature. For example, at 1.0×10^7 seconds of thermal production, the production temperatures of the well are 102.59°C, 83.89°C, 62.89°C, and 38.17°C, respectively. At 1.0×10^8 seconds of thermal production, the production temperatures of the well are 33.19°C, 29.85°C, 27.03°C, and 23.28°C, respectively. Therefore, as time progresses, the rate of decrease in the production temperature will gradually increase.

Based on the aforementioned research results, we compared the thermal-hydromechanical coupled model constructed by Xue et al. [44] in the same field. This model studied the formation and development of fractures in hot dry rock reservoirs during hydraulic fracturing. Through numerical simulations and laboratory experiments, Xue et al. explored the temperature and stress fields between water-cooling impacts and high-temperature rock. Both our numerical model and Xue et al.'s numerical model found that when injecting low-temperature water, it disturbs the

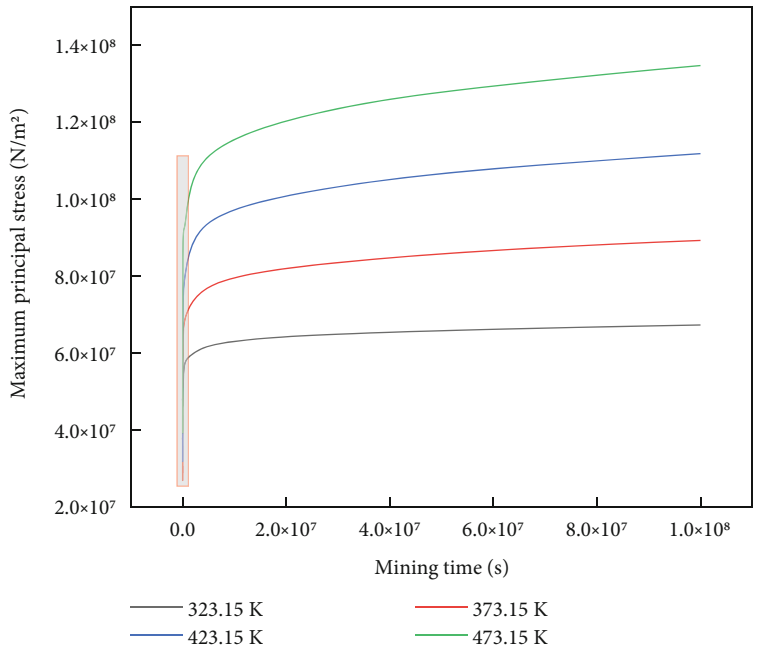

Figure 23: Maximum principal stress maps at different initial reservoir temperatures.

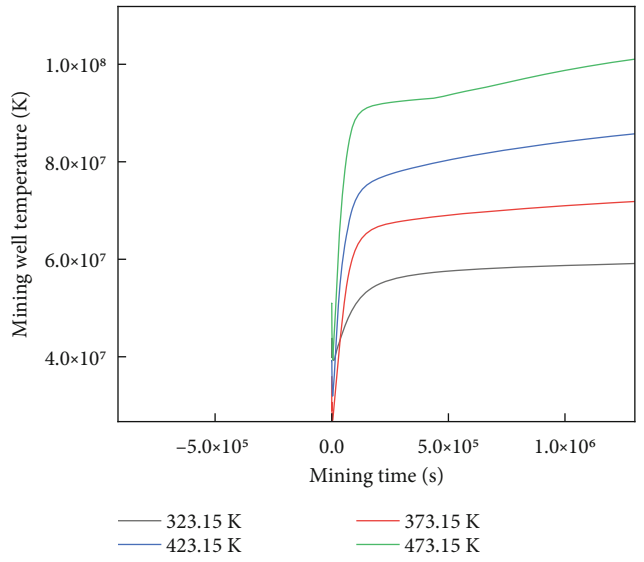

Figure 24: Local magnification of maximum principal stress at different initial reservoir temperatures.

temperature and pressure distribution of the wellbore surrounding rock, resulting in the generation of thermal stress and pore water pressure. The temperature differences caused by thermal stress and the degradation of mechanical parameters of high-temperature rock caused by water cooling impacts will affect the stress field of hot dry rock reservoirs. The changes in the stress field can cause rock damage and increase the rock's permeability. Temperature variations also alter the physical properties of the fluid. Therefore, to achieve optimization in enhanced geothermal systems (EGS), we should consider multiple factors simultaneously, including the in situ stress, initial temperature of the rock, and injection water pressure.

Furthermore, our constructed numerical model, while having many advantages in exploring enhanced geothermal systems (EGS), also has limitations and uncertainties. The calculation results of the numerical model rely on the establishment of reasonable assumptions and simplifications of the system, including the physical parameters of the rock reservoir and the geometric morphology of the fracture network. However, in real-world scenarios, the stress and temperature fields are often more complex, making it possible that these assumptions may not fully conform to actual conditions, thereby affecting the accuracy of the results. Therefore, in practical applications, it is important to fully consider factors such as model assumptions, parameter

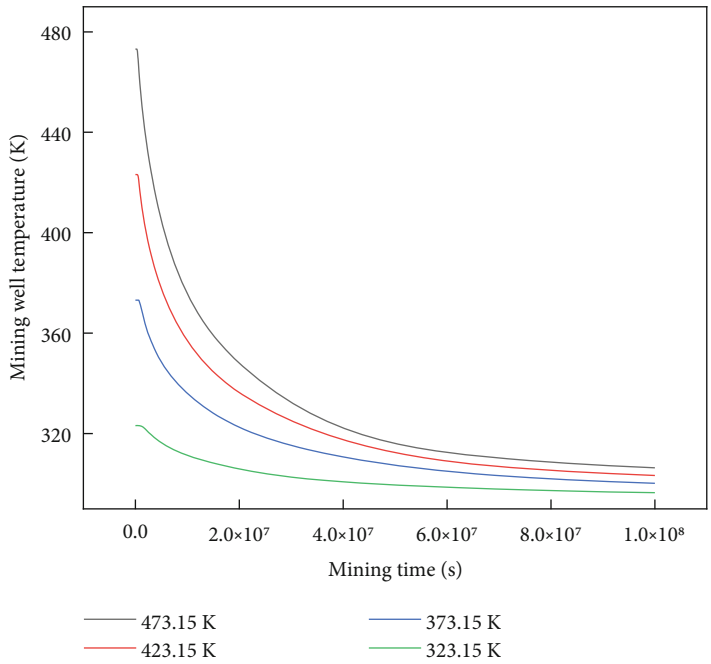

Figure 25: Production well temperature maps at different initial reservoir temperatures.

estimation errors, and the applicability range of the results in order to better evaluate the reliability of the simulation results and provide guidance for further research and application.

4. Conclusion

In this study, the spatiotemporal evolution of the temperature field, stress field, and flow field in the enhanced geothermal system (EGS) reservoir is analyzed under the combined influence of matrix rock and fractures using a developed fractured rock heat transfer model. Additionally, the impacts of various factors such as injection water temperatures, injection-production pressure differentials, reservoir initial temperatures, and injection rates on the heat transfer process of EGS are investigated. The key findings can be summarized as follows:

(1) Considering the thermal-fluid-solid coupling effect is crucial in the operation of enhanced geothermal systems (EGS), as it involves the interplay and mutual influence among the flow field, temperature field, and stress field. During the process of heat extraction, the advantages of the local flow field become evident, with low-temperature working fluid preferentially flowing within dominant flow areas within fractures. This leads to the expansion of these dominant areas and the gradual reduction of weaker areas, resulting in an uneven distribution of the three fields. Furthermore, the heat extraction efficiency near fractures is high, whereas it is low at the periphery of the rock mass. This situation is unfavorable for improving the overall heat extraction performance and reducing the total heat extraction rate of the reservoir. Therefore, enhancing the heat extraction performance of the EGS system requires considering the mutual influence of the three fields and improving heat extraction in the peripheral area of the reservoir to achieve effective utilization of the entire reservoir

(2) The injection-production pressure differential has a significant impact on the flow velocity and heat transfer capacity of water. It determines the flow direction of water within the reservoir. A larger pressure differential leads to higher water velocity and heat transfer capacity within the reservoir, resulting in faster heat exchange and transfer. Meanwhile, an appropriate pressure differential can ensure the heat extraction efficiency and exploitation lifespan. This is because the optimal pressure differential allows the water velocity and heat transfer capacity within the reservoir to reach a reasonable level, thus effectively extracting the heat energy within the reservoir. This avoids the waste of reservoir energy and the loss of resources, improves the heat extraction efficiency and economic benefits of the reservoir, and extends its service life

(3) The injection water temperature affects the temperature difference between the fluid and fractured rock. A lower injection water temperature results in a larger temperature difference, leading to a more intense heat transfer process and a higher heat output. The injection water temperature also influences the production temperature, as higher injection water temperatures result in higher production temperatures. In addition, increasing the injection water temperature can effectively delay the occurrence of

thermal breakthrough and prolong the operation life of the system. Therefore, in practical engineering, the injection water temperature should be adjusted based on specific conditions to balance the performance of the system, production temperature, and lifespan

(4) Raising the injection rate can enhance heat extraction efficiency while simultaneously reducing the sustainable production duration of the reservoir. Therefore, in practical engineering, an appropriate injection rate should be chosen to ensure efficient heat extraction and reservoir lifespan

(5) A higher initial reservoir temperature has a positive correlation with increased production temperature and enhanced heat extraction capacity of the EGS system. However, it is important to note that elevating the initial reservoir temperature also raises the potential for seismic hazards. This is because a higher initial temperature reduces the strength and stability of the reservoir rock mass, making it prone to dynamic phenomena such as fracturing, sliding, and collapse, causing damage and failure of the reservoir. These dynamic phenomena have implications on both the heat extraction efficiency and lifespan of the reservoir, as well as the potential for seismic hazards, posing risks to the safety of personnel and equipment. Thus, raising the initial temperature of the reservoir corresponds to an increased risk of seismic hazards. It is necessary to balance the heat extraction efficiency and reservoir stability, choose an appropriate initial temperature, and achieve sustainable development and optimal utilization of the reservoir

This study explores in detail the impact of water injection temperature, injection-production pressure differential, injection flow rate, and initial reservoir temperature on the heat recovery process in enhanced geothermal systems (EGS) through sensitivity analysis. By numerical simulation, the coupling effects between the permeation field, stress field, and temperature field in fractured rock masses are comprehensively analyzed. The study suggests that increasing the injection water temperature and injection-production pressure differential can enhance the heat recovery capacity of the reservoir but may also accelerate thermal breakthrough and reduce the system's operating life. Increasing the injection flow rate can improve heat recovery efficiency, but too much injection flow rate can cause other problems in the reservoir. Raising the reservoir temperature can lead to higher output temperature, which may cause dynamic disasters. Therefore, while ensuring the efficiency of the system's heat recovery, the lifespan of the EGS can be extended by adjusting the water injection temperature in stages, setting a reasonable injection-production pressure differential, and selecting a suitable injection flow rate to achieve optimization.

Data Availability

The data used to support the findings of this study are included within the article.

Conflicts of Interest

The authors declare that they have no conflicts of interest.

Acknowledgments

The authors are grateful to the financial support from the National Natural Science Foundation of China (52204112, 12002270, 52274096, and 42007264); the Key Research and Development Program of Shaanxi Province, China (2022ZDLSF07-06 and 2023-YBSF-369); the Natural Science Basic Research Program of Shaanxi (2022JM-216 and 2022JC-LHJJ-08); and the Scientific Research Program Funded by Shaanxi Provincial Education Department (No. 22JK0480).

References

[1] J. B. Smith, "From global to regional climate change: relative knowns and unknowns about global warming," *Fisheries*, vol. 15, no. 6, pp. 2–6, 1990.

[2] J. Han, J. Wang, D. Jia et al., "Construction technologies and mechanical effects of the pipe-jacking crossing anchor-cable group in soft stratum," *Frontiers in Earth Science*, vol. 10, article 1019801, 2023.

[3] M. F. Vigoya, J. G. Mendoza, and S. O. Abril, "International energy transition: a review of its status on several continents," *International Journal of Energy Economics and Policy*, vol. 10, no. 6, pp. 216–224, 2020.

[4] I. B. Fridleifsson, "Geothermal energy for the benefit of the people," *Renewable and Sustainable Energy Reviews*, vol. 5, no. 3, pp. 299–312, 2001.

[5] X. G. Zhao and G. Wan, "Current situation and prospect of China's geothermal resources," *Renewable and Sustainable Energy Reviews*, vol. 32, pp. 651–661, 2014.

[6] L. Wang, Y. Xue, Z. Cao, X. J. Wu, F. N. Dang, and R. Liu, "Mechanical properties of high-temperature granite under liquid nitrogen cooling," *Geofluids*, vol. 2023, Article ID 3819799, 23 pages, 2023.

[7] T. Li, W. Zhao, R. Liu, J. Y. Han, P. Jia, and C. Cheng, "Visualized direct shear test of the interface between gravelly sand and concrete pipe," *Canadian Geotechnical Journal*, 2023.

[8] L. Shen and L. Liu, "China's geothermal resources development status, problems and suggestions under the background of carbon neutrality," *IOP Conference Series: Earth and Environmental Science*, vol. 766, no. 1, article 012018, 2021.

[9] K. Menberg, F. Heberle, C. Bott, D. Brüggemann, and P. Bayer, "Environmental performance of a geothermal power plant using a hydrothermal resource in the southern German Molasse Basin," *Renewable Energy*, vol. 167, pp. 20–31, 2021.

[10] Y. C. Guo, G. Cheng, K. Hu, and P. Y. Wang, "Analysis of HDR power generation technology," *Advanced Materials Research*, vol. 616-618, pp. 1128–1132, 2013.

[11] Z. X. Sun, X. Zhang, Y. Xu et al., "Numerical simulation of the heat extraction in EGS with thermal-hydraulic-mechanical coupling method based on discrete fractures model," *Energy*, vol. 120, pp. 20–33, 2017.

[12] L. Wang, Y. Xue, Z. Cao, H. Kong, J. Han, and Z. Zhang, "Experimental study on mode I fracture characteristics of granite after low temperature cooling with liquid nitrogen," *Water*, vol. 15, no. 19, p. 3442, 2023.

[13] J. Han, J. Wang, C. Cheng et al., "Mechanical response and parametric analysis of a deep excavation structure overlying an existing subway station: a case study of the Beijing subway station expansion," *Frontiers in Earth Science*, vol. 10, article 1079837, 2023.

[14] Q. Li, Y. Han, X. Liu, U. Ansari, Y. Cheng, and C. Yan, "Hydrate as a by-product in CO2 leakage during the long-term sub-seabed sequestration and its role in preventing further leakage," *Environmental Science and Pollution Research*, vol. 29, no. 51, pp. 77737–77754, 2022.

[15] Q. Li, F. Wang, Y. Wang et al., "Experimental investigation on the high-pressure sand suspension and adsorption capacity of guar gum fracturing fluid in low-permeability shale reservoirs: factor analysis and mechanism disclosure," *Environmental Science and Pollution Research*, vol. 29, no. 35, pp. 53050–53062, 2022.

[16] F. Wang, Z. Xiao, X. Liu et al., "Strategic design of cellulose nanofibers@ zeolitic imidazolate frameworks derived mesoporous carbon-supported nanoscale $CoFe_2O_4$/CoFe hybrid composition as trifunctional electrocatalyst for Zn-air battery and self-powered overall water-splitting," *Journal of Power Sources*, vol. 521, article 230925, 2022.

[17] Y. Wang, X. Liu, and Y. Xiong, "Numerical simulation of zonal disintegration of surrounding rock in the deep-buried chamber," *Deep Underground Science and Engineering*, vol. 1, no. 2, pp. 174–182, 2022.

[18] Z. Sun, Y. Xin, J. Yao et al., "Numerical investigation on the heat extraction capacity of dual horizontal Wells in enhanced geothermal systems based on the 3-D THM model," *Energies*, vol. 11, no. 2, p. 280, 2018.

[19] S. M. Lu, "A global review of enhanced geothermal system (EGS)," *Renewable and Sustainable Energy Reviews*, vol. 81, pp. 2902–2921, 2018.

[20] Z. Li, X. Hao, Y. Liu, and L. Li, "The mechanism of inward and outward expansion of multiscale dynamic permeability of coalbed methane at different temperatures," *Deep Underground Science and Engineering*, vol. 2, no. 1, pp. 88–101, 2023.

[21] S. Y. Pan, M. Gao, K. J. Shah, J. Zheng, S. L. Pei, and P. C. Chiang, "Establishment of enhanced geothermal energy utilization plans: Barriers and strategies," *Renewable Energy*, vol. 132, pp. 19–32, 2019.

[22] C. Kunze and M. Hertel, "Contested deep geothermal energy in Germany—the emergence of an environmental protest movement," *Energy Research & Social Science*, vol. 27, pp. 174–180, 2017.

[23] O. Kappelmeyer and R. Jung, "HDR experiments at Falkenberg/Bavaria," *Geothermics*, vol. 16, no. 4, pp. 375–392, 1987.

[24] R. Bertani, "Geothermal power generation in the world 2005–2010 update report," *Geothermics*, vol. 41, pp. 1–29, 2012.

[25] K. Mizugaki, "Geologic structure and volcanic history of the Yanaizu-Nishiyama (Okuaizu) geothermal field, Northeast Japan," *Geothermics*, vol. 29, no. 2, pp. 233–256, 2000.

[26] T. Koseki, "Geothermal features of Yamagata prefecture, Northeast Japan 2010," in *Proceedings of the World geothermal congress*, Bali, Indonesia, April 2010.

[27] R. Baria, J. Baumgärtner, A. Gérard, R. Jung, and J. Garnish, "European HDR research programme at Soultz-sous-Forêts (France) 1987–1996," *Geothermics*, vol. 28, no. 4-5, pp. 655–669, 1999.

[28] J. W. Tester, B. J. Anderson, A. S. Batchelor et al., "Impact of enhanced geothermal systems on US energy supply in the twenty-first century," *Philosophical Transactions of the Royal Society A: Mathematical, Physical and Engineering Sciences*, vol. 365, no. 1853, pp. 1057–1094, 2007.

[29] S. P. Hunt and C. Morelli, *Cooper Basin HDR Hazard Evaluation: Predictive Modeling of Local Stress Changes due to HFR Geothermal Energy Operations in South Australia*, University of Adelaide Report Book, 2006.

[30] X. Song, Y. Shi, G. Li et al., "Numerical simulation of heat extraction performance in enhanced geothermal system with multilateral wells," *Applied Energy*, vol. 218, pp. 325–337, 2018.

[31] Y. Zhao, Z. Feng, Z. Feng, D. Yang, and W. Liang, "THM (Thermo-hydro-mechanical) coupled mathematical model of fractured media and numerical simulation of a 3D enhanced geothermal system at 573 K and buried depth 6000–7000 M," *Energy*, vol. 82, pp. 193–205, 2015.

[32] A. Borgia, K. Pruess, T. J. Kneafsey, C. M. Oldenburg, and L. Pan, "Numerical simulation of salt precipitation in the fractures of a CO_2-enhanced geothermal system," *Geothermics*, vol. 44, pp. 13–22, 2012.

[33] S. Zhang, Z. Li, Y. Xu, and C. Zhang, "Three-dimensional numerical simulation and analysis of fluid-heat coupling heat-transfer in fractured rock mass," *Rock and Soil Mechanics*, vol. 32, no. 8, pp. 2507–2511, 2011.

[34] B. G. Chen, E. X. Song, and X. H. Cheng, "A numerical method for discrete fracture network model for flow and heat transfer in two-dimensional fractured rocks," *Chinese Journal of Rock Mechanics and Engineering*, vol. 33, no. 1, pp. 43–51, 2014.

[35] F. Jiang, L. Luo, and J. Chen, "A novel three-dimensional transient model for subsurface heat exchange in enhanced geothermal systems," *International Communications in Heat and Mass Transfer*, vol. 41, pp. 57–62, 2013.

[36] A. R. Shaik, S. S. Rahman, N. H. Tran, and T. Tran, "Numerical simulation of fluid-rock coupling heat transfer in naturally fractured geothermal system," *Applied Thermal Engineering*, vol. 31, no. 10, pp. 1600–1606, 2011.

[37] R. Baria, J. Baumgärtner, F. Rummel, R. J. Pine, and Y. Sato, "HDR/HWR reservoirs: concepts, understanding and creation," *Geothermics*, vol. 28, no. 4-5, pp. 533–552, 1999.

[38] Y. Wang, T. Li, Y. Chen, and G. Ma, "A three-dimensional thermo-hydro-mechanical coupled model for enhanced geothermal systems (EGS) embedded with discrete fracture networks," *Computer Methods in Applied Mechanics and Engineering*, vol. 356, pp. 465–489, 2019.

[39] P. Asai, P. Panja, J. McLennan, and M. Deo, "Effect of different flow schemes on heat recovery from enhanced geothermal systems (EGS)," *Energy*, vol. 175, pp. 667–676, 2019.

[40] D. W. Brown, "A hot dry rock geothermal energy concept utilizing supercritical CO_2 instead of water," *Proceedings of the twenty-fifth workshop on geothermal reservoir engineering*, , pp. 233–238, Stanford University, 2000.

[41] K. Pruess, "Enhanced geothermal systems (EGS) using CO_2 as working fluid—a novel approach for generating renewable energy with simultaneous sequestration of carbon," *Geothermics*, vol. 35, no. 4, pp. 351–367, 2006.

[42] K. Pruess, "On production behavior of enhanced geothermal systems with CO_2 as working fluid," *Energy Conversion and Management*, vol. 49, no. 6, pp. 1446–1454, 2008.

[43] K. Pruess, "Formation dry-out from CO_2 injection into saline aquifers: 2. Analytical model for salt precipitation," *Water Resources Research*, vol. 45, no. 3, 2009.

[44] Y. Xue, S. Liu, J. Chai et al., "Effect of water-cooling shock on fracture initiation and morphology of high-temperature granite: application of hydraulic fracturing to enhanced geothermal systems," *Applied Energy*, vol. 337, article 120858, 2023.